

THE TEMPERATURE DEPENDENCE OF THE
FERROMAGNETIC RESONANCE
LINE WIDTH IN SINGLE
CRYSTALS OF IRON AND NICKEL

Thesis for the Degree of Ph. D.
MICHIGAN STATE COLLEGE
Jerry Arnold Cowen
1954



3 1293 01764 0339

This is to certify that the

thesis entitled

The Temperature Dependence of the
Ferromagnetic Resonance Line Width
in Single Crystals of Iron and Nickel

presented by

Jerry A. Cowen

has been accepted towards fulfillment
of the requirements for

Ph D degree in Physics

R.D. Spence

Major professor

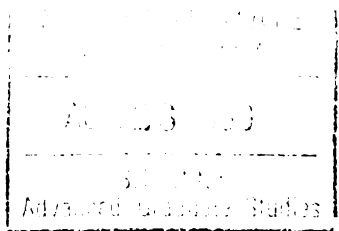
Date March 22 1954



PLACE IN RETURN BOX to remove this checkout from your record.
TO AVOID FINES return on or before date due.
MAY BE RECALLED with earlier due date if requested.

| DATE DUE | DATE DUE | DATE DUE |
|----------|----------|----------|
| 07-11-13 | | |
| | | |
| | | |
| | | |
| | | |
| | | |
| | | |
| | | |
| | | |
| | | |
| | | |

ABSTRACT



The temperature dependence of the Ferromagnetic Resonance Line Width in single crystals of Iron and Nickel

J.A. Cowen

The temperature dependence of the ferromagnetic resonance absorption in single crystals of iron and nickel has been measured from room temperature to the Curie point. The g factor and line width were measured and the line width interpreted in terms of a reciprocal parameter $1/T_2$.

$1/T_2$ remains essentially constant from room temperature to near the Curie point of the nickel (350°C) with a value of approximately $5 \times 10^9 \text{ sec}^{-1}$. Near the Curie point it appears to rise very rapidly but since the calculated value depends on accurate determination of the saturation magnetization which is strongly temperature dependent, the effect may not be real. In iron $1/T_2$ remained constant at approximately $10 \times 10^9 \text{ sec}^{-1}$ up to 750°C . The data was taken using several different orientations of the single crystals and also using polycrystalline samples—each sample gave essentially the same results.

THE TEMPERATURE DEPENDENCE OF THE
FERROMAGNETIC RESONANCE LINE WIDTH IN SINGLE
CRYSTALS OF IRON AND NICKEL

by
JERRY ARNOLD COWEN

A THESIS

Submitted to the School of Graduate Studies of Michigan
State College of Agriculture and Applied Science
in partial fulfillment of the requirements
for the degree of
DOCTOR OF PHILOSOPHY
Department of Physics and Astronomy

1954

10524
12513

ACKNOWLEDGMENTS

The author wishes to thank Professor R. D. Spence for his ever helpful suggestions and his constant interest. Truly, the work would never have been performed without the encouragement and many hours of assistance which he gave.

He is also indebted to Professor A. J. Smith of the Department of Metallurgical Engineering for his suggestions on the metallurgical phase of the work and for the use of the facilities of his department. To Mr. C. Kingston for his patient help with the machine work involved and to Mr. Joe Mudar whose help and good humor lightened the load immeasurably, many thanks are due.

VITA

Jerry Arnold Cowen

candidate for the degree of

Doctor of Philosophy

Final examination: March 22, 1954, 10:00 A. M., Physics
Conference Room

Dissertation: The Temperature Dependence of the Ferro-
magnetic Resonance Line Width in Single
Crystals of Iron and Nickel

Outline of Studies

Major Subject: Physics
Minor Subject: Mathematics

Biographical Items

Born: July 17, 1924, Toledo, Ohio

Undergraduate Studies: Denison University 1942-43
Harvard College 1946-48

Graduate Studies: Michigan State College 1949-54

Experience: Project Engineer, Alden Products Co.,
1948-49; Graduate Assistant, Michigan
State College, 1950-52; Research
Assistant, Michigan State College, 1953;
Assistant Professor, Colorado A & M
College, 1953-54

Member of Sigma Xi, American Association of Physics
Teachers, American Physical Society

TABLE OF CONTENTS

| | Page |
|--|------|
| I. INTRODUCTION | 1 |
| II. THEORY | |
| a. Energy Absorption in a Magnetic Conductor | 7 |
| b. Ferromagnetic Resonance Absorption in an Isotropic Medium | 10 |
| c. Ferromagnetic Resonance Absorption in Anisotropic Media | 15 |
| III. THEORY OF THE USE OF THE RESONANT CAVITY | 20 |
| IV. EXPERIMENTAL METHOD | |
| a. Microwave Apparatus | 25 |
| b. Mounting of Samples | 27 |
| c. Heating of Samples | 30 |
| d. The Magnet | 31 |
| e. Preparation of Samples | 34 |
| f. Electrolytic Polishing | 36 |
| g. Domain Structure | 39 |
| V. ANALYSIS OF RESULTS | 41 |
| VI. RESULTS AND CONCLUSIONS | |
| a. Nickel | 50 |
| b. Iron | 59 |
| c. Conclusions | 69 |
| LIST OF REFERENCES CITED | |

LIST OF FIGURES

| | Page |
|---|------|
| Figure 1. Precessing Magnetic Dipole in a Large Static and Small R-F Magnetic Field | 2 |
| Figure 2. Motion of the Magnetization Vector in Ferromagnetic Resonance | 11 |
| Figure 3. Diagram Illustrating Anisotropy Torque | 18 |
| Figure 4. Equivalent Circuit of Resonant Cavity | 20 |
| Figure 5. Block Diagram of Apparatus | 26 |
| Figure 6. Cavity Assembly as used in Anisotropy Measurements | 29 |
| Figure 7. Magnet Calibration Curve | 33 |
| Figure 8. Experimental Apparatus for Electrolytic Polishing of Small Iron Samples | 37 |
| Figure 9. Electrical Characteristics of the Polishing Cell | 37 |
| Figure 10. The Method of Determining H_0^+ and H_0^- from the Experimental Curve $R(H)$ and the Theoretical Curve R^+ and R^- | 44 |
| Figure 11. Normalized Curve for Electroplated Nickel | 51 |
| Figure 12. $H_0 \text{ res}$ as a Function of Angle in the (100) Plane of Nickel | 52 |
| Figure 13. $H_0 \text{ res}$ as a Function of Angle in the (110) Plane of Nickel | 53 |
| Figure 14. Temperature Dependence of $1/T_2$ for Nickel | 55 |
| Figure 15. $1/T_2$ versus Number of Scratches in an 18% Co-Ni Plated Alloy | 58 |
| Figure 16. g Values for Nickel | 60 |

| | |
|--|----|
| Figure 17. H_0 res as a function of Angle in the (100) Plane of Iron | 61 |
| Figure 18. H_0 res as a Function of Angle in the (110) Plane of Iron | 62 |
| Figure 19. Diagram Illustrating Effect of Ani- sotropy Torque at Low Applied Fields | 65 |
| Figure 20. Temperature Dependence of H_0 res for Double Peaks | 66 |
| Figure 21. Temperature Dependence of $1/T_2$ for Iron | 68 |
| Figure 22. Photograph of Apparatus | 72 |
| Figure 23. Photograph of Apparatus | 73 |

THE TEMPERATURE DEPENDENCE OF THE FERROMAGNETIC RESONANCE LINE WIDTH IN SINGLE CRYSTALS OF IRON AND NICKEL

I. INTRODUCTION

Ferromagnetic resonance absorption can best be understood by consideration of the motion of a single magnetic dipole in an external magnetic field. Consider an essentially free electron with a spin magnetic moment μ . In the presence of a static magnetic field H , it will precess with a frequency $f = \frac{\gamma}{2\pi} H$ known as the Larmor frequency. If a radio frequency magnetic field (of frequency f) is applied to the dipole at right angles to the static field (Fig. 1) the dipole will absorb energy from the radio frequency field with an accompanying increase in the angle θ between the dipole axis and the direction of H .

A ferromagnet can be visualized, in the simplest case, as consisting of a large number of electron spin magnetic moments all strongly coupled together to give a large resultant magnetic moment. In the presence of static and radio frequency fields of the correct magnitude and configuration it will absorb energy from the varying field. Quantum mechanically we say that the static field splits previously degenerate energy levels into levels of magnetic quantum number m_s and that the radio frequency field can excite transitions between

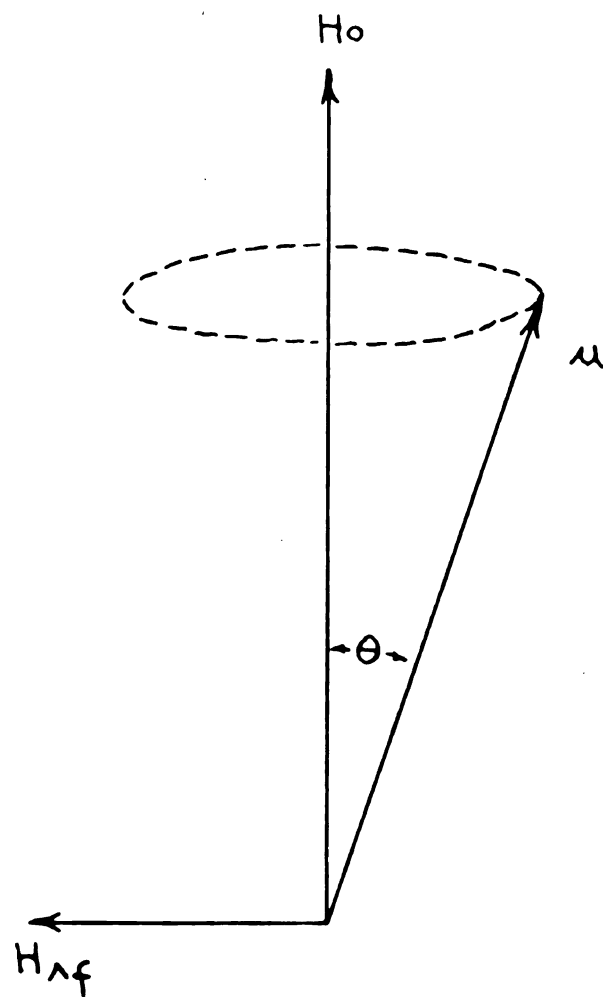


FIG.1 PRECESSING MAGNETIC DIPOLE IN A
LARGE STATIC AND SMALL R-F
MAGNETIC FIELD

these levels so long as the selection rule $\Delta m_s = \pm 1$ is satisfied. The lowest energy level is the most densely populated so that the net effect is an absorptive one. The absorption continues because the spins give up energy to the crystalline lattice tending to maintain an excess of electrons in the lower state. This absorption of radio frequency energy is describable by a change in the radio frequency permeability. Whereas the absorption due to a single dipole occurs at essentially one frequency or value of applied field, the absorption in a ferromagnet is appreciable over a broad range of applied fields, giving rise to a resonance type curve.

The first experimental observations on ferromagnetic resonance absorption were made by Griffiths¹ in 1946. He electroplated thin films of the ferromagnetic elements onto the endplate of a cylindrical microwave resonant cavity. The static magnetic field was applied parallel to this surface and the cavity was excited in such a manner that the radio frequency magnetic field was parallel to the endplate and also perpendicular to the static field. He then measured the Q of the cavity as a function of the applied field and observed a broad resonance type curve.

A short time later Yager and Bozorth² observed the absorption in sheets of Superalloy and in 1948 Kip and Arnold³ made measurements on the absorption as a function of the orientation of a 3% silicon iron single crystal

A few other papers have been published on resonance in metals,^{4,5} the most complete of which was the work of Bloembergen⁶ on the temperature dependence of the resonance position and line width in polycrystalline Nickel and supermalloy.

During this period several workers⁷⁻¹⁰ were investigating the temperature and anisotropy dependence of the resonance line in various ferrites. These materials are magnetic semiconductors of the form $X\text{Fe}_2\text{O}_3$ where X is a metallic bivalent ion. They have high resistivity (compared to the metals) and consequently large skin depth and few conduction electrons. The large skin depth means that samples of reasonable size will be uniformly magnetized by the microwave field, and their lack of conduction electrons presumably simplifies the theoretical calculations.

Because of the simplifications which the ferrites appear to introduce, resonance in metals has been neglected. There have been no measurements on the temperature dependence of the resonance line in single crystals and only the few mentioned above on polycrystalline materials.

The situation with respect to theory is even less satisfactory. Griffiths attempted to interpret his first results by assuming that the magnetic dipoles precessed in the Lorentz field $H = H_0 + \frac{4}{3}\pi M$. The resulting calculated Larmor frequency was small by a factor of about four. Kittel,¹¹ using phenomenological arguments, suggested a modified theory in which the resonant frequency was

given by $f = \frac{\gamma}{2\pi} (B H_0)^{\frac{1}{2}}$ instead of $f = \frac{\gamma}{2\pi} H_0$ as in the Larmor case. This theory, which will be discussed in detail later on, has been very successful in predicting the position of the resonance line as a function of sample shape, anisotropy and temperature. Van Vleck¹² has obtained essentially the same results as Kittel using a quantum mechanical approach - obtaining eigenfrequencies which are the same as Kittel's resonant frequencies.

There have been no satisfactory theoretical explanations of the temperature dependence of the line width. Bloembergen, using relations first employed by Bloch¹³ to discuss the problem of nuclear magnetic resonance, was able to represent the line width by means of a spin-spin relaxation time and a spin-lattice relaxation time. Abrahams and Kittel¹⁴ calculated the temperature dependence of the spin-lattice relaxation time by considering that the radio frequency field excited spin waves and assuming that the spin system itself came to equilibrium before the spin lattice transition had time to proceed. Unfortunately, it is commonly assumed that the principal contribution to the line width comes from the spin-spin terms and there have been no theoretical calculations on their temperature dependence. Kittel and Abrahams¹⁵ have suggested that although at temperatures below one-half of the Curie temperature the spin-spin terms do predominate, at temperatures higher than this the spin-lattice terms take over. If this is so then the assumption that the spin-spin terms make the major contribution may be in error.

The object of the present work was to measure the temperature dependence of the ferromagnetic resonance absorption line width in single crystals and polycrystalline samples of iron and nickel from room temperature to the respective Curie temperatures and thus obtain information on the mechanism responsible for line width and the effect of anisotropy on the line width. It was hoped that this would present a more complete picture of resonance in metals and lead to a more satisfactory theory of ferromagnetic resonance.

II. THEORY

a. Energy Absorption in a Magnetic Conductor

Before considering the theory of ferromagnetic resonance absorption, it will prove useful to derive the equations for the energy absorbed by a ferromagnetic conductor from an radio frequency field and to show that this can be expressed in terms of an effective permeability μ_{eff} .¹⁶

In the Gaussian system of units, Maxwell's equations are given by:

$$\begin{array}{ll} \text{A) } \nabla \times \underline{H} = \frac{1}{c} (4\pi \underline{J} + \dot{\underline{D}}) & \text{C) } \nabla \cdot \underline{D} = 4\pi \rho \\ \text{B) } \nabla \times \underline{E} = -\frac{1}{c} \dot{\underline{B}} & \text{D) } \nabla \cdot \underline{B} = 0 \end{array} \quad 2-1$$

with the constitutive relations $\underline{B} = \mu \underline{H}$; $\underline{D} = \epsilon \underline{E}$; $\underline{J} = \sigma \underline{E}$.

Assuming that the field quantities vary in a sinusoidal manner with the frequency ω , (A) and (B) reduce to

$$\begin{aligned} c \nabla \times \underline{H} &= (4\pi\sigma + j\omega\epsilon) \underline{E} \\ c \nabla \times \underline{E} &= -j\omega\mu \underline{H} \end{aligned} \quad 2-2$$

$$\text{From this it can be shown: } \nabla^2 \underline{H} = K^2 \underline{H} \quad 2-3$$

$$\text{where } K^2 = \frac{(4\pi i\sigma\omega\mu - \omega^2\epsilon\mu)}{c^2}$$

In general both μ and ϵ may be complex, $\mu = \mu_1 - j\mu_2$; $\epsilon = \epsilon_1 - j\epsilon_2$. By assuming the characteristic dimension of the conductor (in this case the thickness) small compared to the wave

length in vacuum, the sample can be considered to be in a uniform field H_0 , where H_0 is the amplitude of the time varying field. The field outside the sample satisfies Equation 2-3 with $K_i = 0$.

Consider an infinite sheet of thickness $2d$, then the solution inside is $H_{in} = A_1 \sinh K_i y + A_2 \cosh K_i y$.

The boundary conditions are

$$(H_{in})_{tan} = (H_{out})_{tan}$$

$$(\mu H_{in})_{nor} = (\mu H_{out})_{nor}$$

thus at $y = \pm d$, $H_{in} = H_{out}$

at $y = d$ $H_{out} = A_1 \sinh K_i d + A_2 \cosh K_i d$

at $y = -d$ $H_{out} = -A_1 \sinh K_i d + A_2 \cosh K_i d$

Solving the above equations for A_1 and A_2 , we find

$$A_1 = 0, \quad A_2 = \frac{H_0}{\cosh K_i d}$$

$$H_{in} = \frac{H_0}{\cosh K_i d} \cosh K_i y$$

2-4

also

$$\nabla \times \underline{E} = -\frac{1}{c} \frac{\partial \underline{B}}{\partial t}$$

$$\nabla \times \underline{E}_{in} = -\frac{j\omega\mu}{c} \frac{H_0}{\cosh K_i d} \cosh K_i y$$

$$\underline{E}_{in} = -\frac{j\omega\mu}{K_i c} \frac{H_0}{\cosh K_i d} \sinh K_i y$$

2-5

The energy absorbed is given by

$$\omega = \frac{1}{2} \iiint [\sigma + \omega\epsilon_2) \underline{E} \underline{E}^* + \omega\mu_2 \underline{H} \underline{H}^*] dV$$

$$\omega = \frac{c}{8\pi} \iint \text{Re} (\underline{E} \times \underline{H}^*) ds$$

2-6

Therefore in this case the power absorbed per unit area from one side of the sample is

$$\omega = \operatorname{Re} \left(\frac{j \omega \mu}{8 \pi K_i} H_o^2 \tanh K_i d \right) \quad 2-7$$

For a ferromagnetic metal as used in the resonance experiments $|K|d \gg 1$ and therefore the hyperbolic function can be replaced by 1 resulting in $\omega = \operatorname{Re} \left(\frac{j \omega \mu}{8 \pi K_i} H_o^2 \right)$

for the power flowing into one side of the metal. In a metal the displacement currents are much smaller than the conduction currents and therefore the ϵ term in K_i may be dropped giving

$$\begin{aligned} \omega &= \operatorname{Re} \left(\frac{j \omega \mu \epsilon H_o^2}{8 \pi \sqrt{4 \pi j \omega \mu \sigma}} \right) \\ &= \frac{1}{8 \pi} \frac{H_o^2 \epsilon \omega^{1/2}}{\sqrt{4 \pi \sigma}} \operatorname{Re} \left(\frac{j \mu}{\sqrt{j \mu}} \right) \end{aligned}$$

Let us define an effective permeability $\mu_{\text{eff}} = \mu' + j \mu''$ such that

$$\sqrt{j \mu} = \sqrt{j \mu_1 + \mu_2} = \frac{1}{\sqrt{2}} (\mu_1'^{1/2} + j \mu_1''^{1/2}) \quad 2-8$$

therefore

$$\omega = \frac{1}{8 \pi} \frac{H_o^2 \epsilon \omega^{1/2}}{\sqrt{8 \pi \sigma}} \mu_1'^{1/2}$$

The ferromagnetic resonance experiment measures a quantity proportional to ω . It is also of interest to ask how μ_1 and μ_2 are related to μ' and μ'' ; solving Equation 2-8 one obtains

$$\mu' = \sqrt{\mu_1'^2 + \mu_2^2} + \mu_2 \quad 2-9a$$

$$\mu'' = \sqrt{\mu_1'^2 + \mu_2^2} - \mu_2 \quad 2-9b$$

b. Ferromagnetic Resonance Absorption in an Isotropic Medium

Consider a thin sheet of ferromagnetic material, lying in the xy plane, which is subjected to a large static magnetic field in the z direction and a small radio frequency magnetic field in the x direction (Fig. 2). The magnetization vector will consist of two parts, a large constant M_z and a small varying M_{xy} . The magnetization is related to the total angular momentum by

$$M = \gamma J \quad 2-10$$

where $\gamma = \frac{ge}{\hbar mc}$, g is the spectroscopic splitting factor, e and m are the charge and mass of the electron and c is the velocity of light. The equation of motion is

$$\frac{dJ}{dt} = \text{Total Torque} \quad 2-11$$

In the case of an isotropic ferromagnetic material the torque is just $\underline{M} \times \underline{H}^e$ where \underline{H}^e is the effective field inside the material, that is, the applied field corrected in a suitable manner for the demagnetization effects. The presence of ferromagnetic anisotropy will introduce an additional torque which must be added to that already present. In order to simplify the argument the anisotropy will be neglected for the present.

The components of H^e can be given by an expression of the form $H_j^e = H_j - N_j M_j$ where H_j are the components of the applied field, M_j are the components of the magnetization, and N_j are the demagnetization factors which depend on the shape of the sample. These factors have rigorous meaning only when the sample is ellipsoidal

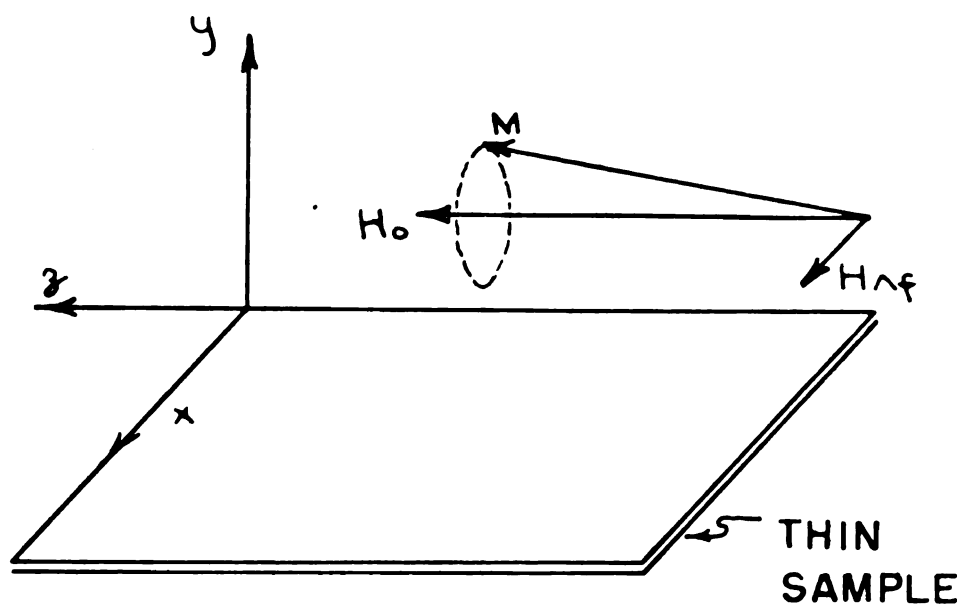


FIG. 2 MOTION OF THE MAGNETIZATION VECTOR. IN FERROMAGNETIC RESONANCE

and when the applied field lies along one of the principal axes of the figure; for only in this case is the internal field uniform and parallel to the applied field.

In this experiment there are demagnetization factors of two types, static and radio frequency. For the static field which penetrates the sample uniformly, Osborne¹⁷ has shown that $H_z^e = H_z - N_z M_z$ where $N_z = \frac{\pi^2}{m} \left(1 - \frac{4}{\pi m}\right)$

for large m . Here m is the ratio of the diameter of the spheroid to its thickness; thus $N_z \simeq \frac{\pi^2}{m}$. For the radio frequency field which penetrates only very slightly into the sample,

$$H_x^e = H_x - N_x M_x$$

$$H_y^e = - N_y M_y$$

where M_x and M_y are the radio frequency components of the magnetization and $N_x = \frac{\pi^2}{m'}$, $N_y = 4\pi \left(1 - \frac{\pi}{2m'} + \frac{2}{m'^2}\right)$

Here m' is the ratio of the diameter to the effective thickness. The thickness is of the order of magnitude of the skin depth $\delta = \sqrt{\frac{2}{\omega \mu \sigma}}$ and therefore $N_x \simeq 0$ and $N_y \simeq 4\pi$.

If one were to solve the equations of motion as they stand in terms of H_x and M_x for a radio frequency susceptibility as a function of frequency, the solution would be essentially monochromatic. Since the resonance lines do have width, damping terms must be added to account for this width. We will, following Bloembergen⁶, use the notation and formalism which was applied by Bloch to the case of nuclear resonance.

There are two types of interactions which can broaden the resonance lines (still considering only isotropic media), those which change the total energy of the spin system and those which can only modify the various components without changing the total energy. In the first class are thermal agitation and spin-orbit interactions. These may be represented as a perturbation on M_z , which in the unperturbed state and for large fields will be parallel to H_0 but which may, due to these effects, have components in other directions. If this is so, M_z will approach M_0 with a relaxation time T_1 given by $\dot{M} = - \frac{M_z - M_0}{T_1}$. T_1 is known as the spin-lattice relaxation time.

The other effect is due to the local magnetic fields of neighboring dipoles or to small inhomogeneities in H . We can represent the whole complex of such effects by an effective irregularity in M_z of the order of H' and define $\gamma H' = \frac{1}{T_2}$. Here again the perturbation on M_x or M_y is assumed to decay exponentially with a relaxation time T_2 such that $\dot{M}_x = - \frac{M_x}{T_2}$. T_2 is the relaxation time for all effects disturbing the spin system from within.

Separating the vector equation of motion into its component parts, we have

$$\begin{aligned}\dot{M}_x &= \gamma [\underline{M} \times \underline{H}^e]_x - \frac{M_x}{T_2} \\ \dot{M}_y &= \gamma [\underline{M} \times \underline{H}^e]_y - \frac{M_y}{T_2} \\ \dot{M}_z &= \gamma [\underline{M} \times \underline{H}^e]_z - \frac{M_z - M_0}{T_1}\end{aligned}\tag{2-12}$$

Assuming $|M_z| = |M_0|$ and that all time variations are of

the form $e^{j\omega t}$, one obtains

$$\begin{aligned} j\omega M_x &= \gamma M_y [H_0 + (N_y - N_z) M_0] - \frac{M_x}{T_2} \\ -j\omega M_y &= \gamma \{ M_x [H_0 + (N_x - N_z) M_0] - H_x M_0 \} + \frac{M_y}{T_2} \\ -j\omega M_z &= \gamma M_y [H_x + M_x (N_y - N_x)] \end{aligned} \quad 2-13$$

Solving for $\frac{M_x}{H_x} = \chi_x$, one obtains

$$\chi_x = \frac{M_x}{H_x} = \frac{\gamma^2 M_y M_0 [H_0 + (N_y - N_z) M_0]}{(j\omega + 1/T_2) [M_y (j\omega + 1/T_2) + \gamma (N_x - N_z) M_0] + \gamma^2 H_0 M_0} \quad 2-14$$

where this is the complex radio frequency susceptibility and is related to the permeability by

$$\begin{aligned} 4\pi \chi_1 &= \mu - 1 \\ 4\pi (\chi_1 - j\chi_2) &= \mu_1 - j\mu_2 - 1 \end{aligned}$$

Thus

$$\mu_1 = \frac{4\pi \gamma^2 M_0 [H_0 + (N_y - N_z) M_0] (\omega_0^2 - \omega^2)}{(\omega_0^2 - \omega^2)^2 + 4\omega^2/T_2^2} + 1 \quad 2-15a$$

$$\mu_2 = \frac{4\pi \gamma^2 M_0 [H_0 + (N_y - N_z) M_0] 2\omega/T_2}{(\omega_0^2 - \omega^2)^2 + 4\omega^2/T_2^2} \quad 2-15b$$

where

$$\omega_0^2 = \gamma^2 \{ H_0 + (N_x - N_z) M_0 \} \times \{ H_0 + (N_y - N_z) M_0 \} + \frac{1}{T_2^2} \quad 2-16$$

These expressions for the real and imaginary parts of the permeability can be combined to give the quantity μ' defined in Equation 2-8.

c. Ferromagnetic Resonance Absorption in Anisotropic Media

It can be shown experimentally that single crystals of magnetic materials are anisotropic with respect to an applied magnetic field. In iron, which is a body centered cubic crystal, the $[100]$ directions are most easily magnetized while the $[111]$ directions are hardest to magnetize. If a disk shaped sample of a single crystal is placed in a magnetic field, it will rotate so that the easy direction is parallel to the applied field. This anisotropy torque is expressible in terms of an anisotropy energy and will affect the position and width of the ferromagnetic resonance absorption.

The empirical condition which the anisotropy energy must satisfy is that it have the symmetry of the crystal. The energy is thus defined in terms of a set of experimentally determined constants, the anisotropy constants, and the direction cosines of the angle between the magnetization vector and the crystal axes. Thus for a cubic crystal,

$$E = K_0 + K_1 (\alpha_1^2 \alpha_2^2 + \alpha_2^2 \alpha_3^2 + \alpha_1^2 \alpha_3^2) + K_2 \alpha_1^2 \alpha_2^2 \alpha_3^2 \quad 2-17$$

where the α_i are the direction cosines and K_1 and K_2 are the first and second order anisotropy constants. The odd power terms are not present because they would not satisfy the requirements of cubic symmetry and the terms in α_i^2 and α_i^4 are missing because of the identity in the direction cosines $\alpha_1^2 + \alpha_2^2 + \alpha_3^2 = 1$. For large applied fields the magnetization is approximately parallel

to the applied field and the direction cosines can be expressed in terms of the angle between the applied field and the axes. Consider a disk cut in the (100) plane,

$\alpha_1 = \sin \theta$; $\alpha_2 = \cos \theta$; $\alpha_3 = 0$ where θ is the angle between the [100] direction and H. Then

$$E = K_0 + K_1 \sin^2 \theta \cos^2 \theta$$

The torque is given by $T = - \frac{\partial E}{\partial \theta}$

$$= - \frac{K_1}{2} \sin 2\theta \cos 2\theta = - \frac{K_1}{4} \sin 4\theta$$

A similar analysis for the (110) plane of a cubic crystal gives

$$T = - \frac{K_1}{8} (2 \sin 2\theta + 3 \sin 4\theta) + \frac{K_2}{64} (\sin 2\theta - 4 \sin 4\theta - 3 \sin 6\theta) \quad 2-18$$

In ferromagnetic resonance absorption in iron, nickel, and their alloys the effects of the second order terms are small and therefore have been neglected.

The most direct way to introduce the anisotropy energy into the expressions for ferromagnetic resonance is to add the anisotropy torque to the equations of motion. This involves solving the equations of motion for each case. Kittel¹¹ has suggested an artifice whereby the anisotropy torque is considered as exerted by an internal field H^{anis} with the torque being expressed as $\underline{M} \times \underline{H}^{anis}$. This internal field is represented by demagnetization factors of the form

$$H_x^{anis} = - N_x^{anis} M_x$$

$$H_y^{anis} = - N_y^{anis} M_y$$

2-19

In the absence of the radio frequency field there are two

torques which balance one another - the anisotropy torque

$$T = - \frac{\partial E}{\partial \theta} \text{ and the torque exerted by the applied field } \underline{M} \times \underline{H}_0.$$

We are interested in torques which change the motion of the magnetization vector, that is, torques exerted when the magnetization vector has been displaced by the radio frequency field. Thus (Figure 3) if M is rotated in the x direction through an angle $\Delta \theta$, there will be a torque in the negative y direction

$$\frac{\Delta T_y}{\Delta \theta} = - \frac{\partial^2 E}{\partial \theta^2}$$

$$\Delta T_y = - \frac{\partial^2 E}{\partial \theta^2} \Delta \theta$$

According to our convention this is due to H_x^{anis} and therefore

$$- \frac{\partial^2 E}{\partial \theta^2} \Delta \theta = \Delta T_y = - M_z H_x^{\text{anis}} = M_z N_x^{\text{anis}} M_x$$

but $M_x \approx M_z \Delta \theta$

therefore $\frac{\partial^2 E}{\partial \theta^2} \Delta \theta = M_z^2 N_x^{\text{anis}} \Delta \theta$

For the case in which M_z lies in the (100) plane and

$$T = \frac{K_1}{2} \sin 4\theta, \quad 2K_1 \cos 4\theta = N_x^{\text{anis}} M_z^2$$

then

$$N_x^{\text{anis}} = \frac{2K_1 \cos 4\theta}{M_z^2} \quad 2-20$$

and similarly $N_y^{\text{anis}} = \frac{2K_1 \cos 4\theta}{M_z^2}$

2-21

In the case where M_z lies in the (110) plane a similar analysis (to first order terms) shows

$$N_x^{\text{anis}} = \frac{K_1}{M_0^2} (2 - \sin^2 \theta - 3 \sin^2 2\theta) \quad 2-22$$

$$N_y^{\text{anis}} = \frac{2K_1}{M_0^2} \left(1 - 2 \sin^2 \theta - \frac{3}{8} \sin^2 2\theta \right) \quad 2-23$$

Adding these terms to the equations of motion, we obtain

S-50

S-51

S-55

S-53

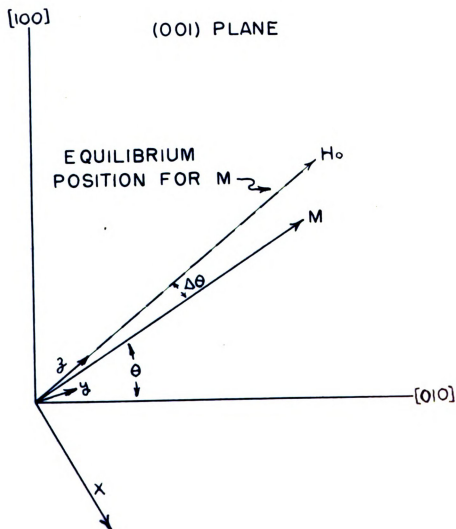


FIG. 3 DIAGRAM ILLUSTRATING ANISOTROPY TORQUE.

$$\begin{aligned}
j\omega M_x &= \gamma [H_0 + (N_y + N_y^a - N_z) M_0] M_y - \frac{M_x}{T_2} \\
j\omega M_y &= \gamma \left\{ [H_0 + (N_x + N_x^a - N_z) M_0] M_x - M_0 H_x \right\} - \frac{M_y}{T_2} \\
j\omega M_z &= \gamma [-H_x + \{N_x + N_x^a - (N_y + N_y^a)\} M_x] M_y \quad 2-24
\end{aligned}$$

Now again solving for the radio frequency permeability μ with the same approximations as before.

$$\mu_1 = \frac{4\pi\gamma^2 M_0 [H_0 + (N_y + N_y^a - N_z) M_0] (\omega_0^2 - \omega^2)}{(\omega_0^2 - \omega^2)^2 + (2\omega/T_2)^2} + 1 \quad 2-25$$

$$\mu_2 = \frac{4\pi\gamma^2 M_0 [H_0 + (N_y + N_y^a - N_z) M_0] 2\omega/T_2}{(\omega_0^2 - \omega^2)^2 + (2\omega/T_2)^2} \quad 2-26$$

where

$$\omega_0^2 = \gamma^2 \left\{ H_0 + (N_x + N_x^a - N_z) M_0 \right\} \times \left\{ H_0 + (N_y + N_y^a - N_z) M_0 \right\} + \frac{1}{T_2^2} \quad 2-27$$

This allows us to formulate the problem for anisotropic media in terms of all of the factors used in the isotropic case and the anisotropy demagnetization terms.

It is of interest to note that this development has assumed that the sample is magnetized to saturation for all values of H_0 . Under certain conditions this assumption is incorrect. Its effect on the resonance curve will be discussed in Section VI b.

III. THEORY OF THE USE OF THE RESONANT CAVITY

A microwave resonant cavity consists of a dielectric filled region completely surrounded by conducting walls except for a small iris or opening. There are electromagnetic field solutions of particular configuration and frequency which satisfy the boundary conditions and correspond to the storage of electromagnetic energy over rather long periods of time. These normal modes, of which there are in general an infinite number, are the resonant frequencies of the cavity. We are interested in only the first few of these for which the linear dimensions of the cavity are of the order of the wave length in the guide.

In analyzing the action of a cavity, the actual cavity parameters can be replaced by an equivalent circuit made up of lumped elements. Thus the cavity and coupling iris may conveniently be replaced by a parallel resonant circuit which is coupled to the transmission line by a transformer. (Figure 4)

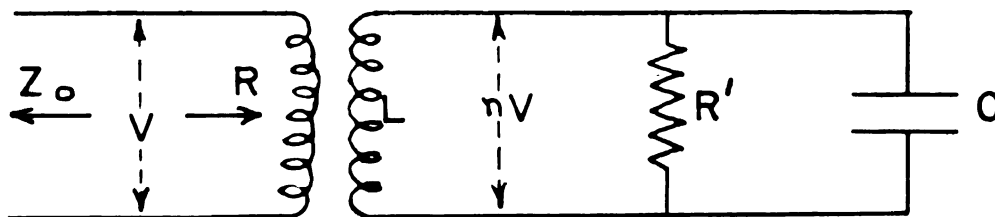


FIG. 4 EQUIVALENT CIRCUIT OF RESONANT CAVITY

We have here assumed that the transmission line is terminated on the left by its characteristic impedance z_0 and that the line sees an effective resistance R on the right. The transformer has a turns ratio n and is assumed to be ideal, that is, there is no energy lost in the transformer. If the cavity is tuned to resonance, from the conservation of energy, $\frac{V^2}{R} = \frac{n^2 V^2}{R'}$, therefore

$$R' = n^2 R \quad 3-1$$

and the impedance which the cavity sees is $z_0' = n^2 z_0$.

The absorbed power is thus

$$\frac{V^2}{R} = \frac{(V_i + V_R)^2}{R} = \frac{V_i^2}{R} (1 + \Gamma^2) \quad 3-2$$

where V is considered to be made up of two components, the voltage of the incident and of the reflected waves on the line, and Γ is the voltage reflection coefficient

$\Gamma = \frac{V_R}{V_i}$. At resonance the load is purely resistive and

$$\Gamma = \frac{R - z_0}{R + z_0}, \text{ thus } \frac{z_0}{R} = \frac{1 - \Gamma}{1 + \Gamma} \quad 3-3$$

Hence at resonance

$$P_a = \frac{V_i^2}{R} (1 + \Gamma^2) = \frac{V_i^2}{z_0} (1 - \Gamma^2) \quad 3-4$$

$$P_i = \frac{V_i^2}{z_0}, \quad P_R = \frac{V_i^2}{z_0} \Gamma^2$$

where P_i , P_a and P_R are the incident, absorbed and reflected powers respectively, and $P_a = P_i - P_R$.

Since both R and z_0 are real numbers, Γ at resonance is real and may be positive or negative. $\frac{1}{n}$ is a measure of the coupling between the cavity and the guide.

We consider two cases depending on whether β_n is large or small.

Case 1

β_n small, undercoupled
 Γ negative, V_R negative

$$V_{max} = V_i - V_R$$

$$V_{min} = V_i + V_R$$

Case 2

β_n large, overcoupled
 Γ positive, V_R positive

$$V_{max} = V_i + V_R$$

$$V_{min} = V_i - V_R$$

3-5

The voltage standing wave ratio ρ is defined $\rho = \frac{V_{max}}{V_{min}}$ and therefore

$$\rho = \frac{V_i - V_R}{V_i + V_R} = \frac{1 - \Gamma}{1 + \Gamma} = \frac{Z_0}{R}$$

$$\rho = \frac{V_i + V_R}{V_i - V_R} = \frac{1 + \Gamma}{1 - \Gamma} = \frac{R}{Z_0} \quad 3-6$$

We now wish to define the Q of the cavity and relate it to the quantities which we usually measure- ρ , $|\Gamma|$, P_R . The total Q is defined as

$$Q_t = 2\pi \frac{\text{energy stored in the cavity}}{\text{total energy lost by the cavity per period}}$$

This total Q_t is made up of two parts, the unloaded Q_u which represents all of the losses in the cavity proper and the external Q_e which represents the energy lost by the cavity to the guide. These are related by

$$\frac{1}{Q_t} = \frac{1}{Q_e} + \frac{1}{Q_u}$$

By considering the energy stored and lost in the equivalent circuits, we can show that $Q_u = \frac{n^2 R}{\omega L}$ and $Q_e = \frac{n^2 Z_0}{\omega L}$

(This is only true if the guide is terminated in its characteristic impedance as it is in this case.) Thus

$$\frac{Q_e}{Q_u} = \frac{Z_0}{R}$$

Q_u is itself made up of two parts, Q_c due to the losses in the copper walls of the cavity excluding the ferromagnetic sample, and Q_{fer} due to the losses in the ferromagnetic sample. These quantities are related in a similar manner by $\frac{1}{Q_u} = \frac{1}{Q_c} + \frac{1}{Q_{fer}}$

The Q_{fer} is primarily due to the magnetic losses in the sample and only very slightly to the eddy current and dielectric losses.

$$Q_{fer} = 2\pi \frac{\text{energy stored in the cavity}}{\text{magnetic energy loss per cycle}}$$

We have shown in section II that the magnetic power loss in a plane sample is proportional to the square root of μ' , the real part of the effective permeability. It has also been shown that μ' is a function of the applied field H . Using these results along with the fact that the other losses in the cavity are independent of H , we obtain $\frac{1}{Q_{fer}} = A' \sqrt{\mu'}$; $\frac{1}{Q_u} = A' \sqrt{\mu'} + B'$

and finally $\frac{Q_c}{Q_u} = A \sqrt{\mu'} + B$ 3-6

We actually measure a power p , proportional to the reflected power, as a function of the applied magnetic field.

$$p = c P_R = c |\Gamma|^2 P_i$$

or $|\Gamma| = \frac{p^{1/2}}{c}$ where $\alpha = \sqrt{c P_i}$

We can determine α by measuring both p and ρ at one point on the curve. For either type coupling, $\rho = \frac{1 + |\Gamma|}{1 - |\Gamma|}$

therefore $|\Gamma| = \frac{\rho-1}{\rho+1}$ and hence $\alpha = \rho^{1/2} \left(\frac{\rho+1}{\rho-1} \right)$ for 3-6a
any point on the curve. Making use of the result ob-
tained earlier that $\frac{Q_e}{Q_u} = \frac{Z_0}{R}$ and also of Equation 3-6
we obtain for the two cases

| undercoupled | overcoupled |
|---|---|
| $A\sqrt{\mu'} + B = \rho = \frac{1 + \Gamma }{1 - \Gamma }$ $= \frac{1 + \frac{\rho^{1/2}}{\alpha}}{1 - \frac{\rho^{1/2}}{\alpha}}$ $= \frac{\alpha + \rho^{1/2}}{\alpha - \rho^{1/2}}$ | $A\sqrt{\mu'} + B = \frac{1}{\rho} = \frac{1 - \Gamma}{1 + \Gamma}$ $= \frac{1 - \frac{\rho^{1/2}}{\alpha}}{1 + \frac{\rho^{1/2}}{\alpha}} \quad 3-7$ $= \frac{\alpha - \rho^{1/2}}{\alpha + \rho^{1/2}}$ |

where A and B involve Q_c and Q_u and are constants for a
given cavity at a given temperature. We have thus shown
that a quantity proportional to the effective permeability
can be obtained from measurements made on the cavity.

IV. EXPERIMENTAL METHOD

a. Microwave Apparatus

The apparatus used in the experiment is of the conventional type as shown in the block diagram (Figure 5). The klystron is a 723AB low power oscillator operating at about 9000 megacycles per second. It is modulated with a 1000 cycle per second square wave which is supplied, along with the necessary DC voltages, from a voltage regulated source. The klystron is isolated from the load by a flap attenuator and these two elements are matched to the H-arm of a magic T with an E-H tuner. The E-arm of the T is connected to a matched detector, the output of which is read on a Browning TAA-16 twin-tee tuned amplifier peaked to match the frequency of the square wave. The two side arms of the T feed the energy to a matched load and to the resonant cavity through a standing wave detector respectively. Energy from the klystron is coupled into the two side arms but not into the E-arm of the T. That portion which goes into the arm containing the matched load is totally absorbed, the other portion is reflected from the cavity and partially coupled into the E arm. Thus, only power which is reflected from the cavity is measured by the detector and the

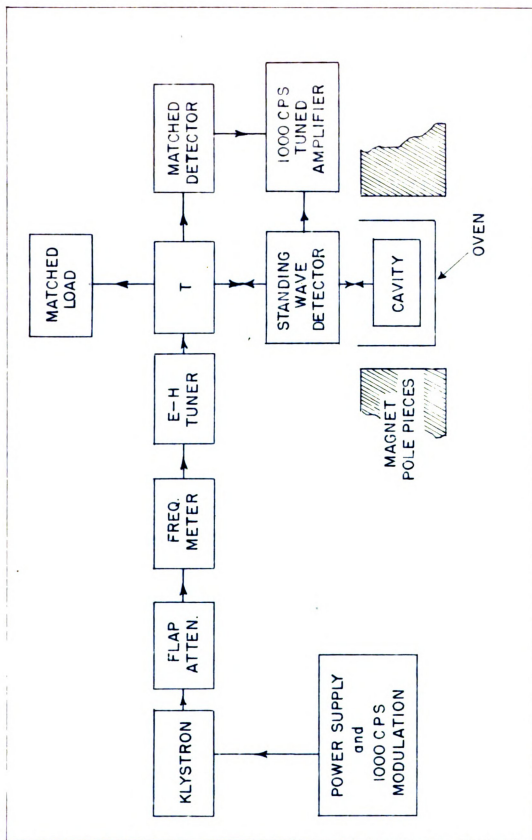


Figure 5 Block diagram of apparatus.

meter reading is proportional to this energy. The matching devices prevent multiple reflections in any of the arms of the T. The overall matching of the system is to a voltage standing wave ratio of about 1.2 except in the arm which contains the cavity, in which the actual standing wave ratio depends on the type of cavity used. A mica window was cemented in the guide to prevent leakage of the hydrogen gas which served as a reducing atmosphere. It was found that the window introduced so little reflection that it was not necessary to match out these reflections with a tuning device.

The cavity used was three half wave lengths long and was coupled to the guide with a circular iris symmetrically placed. An iris with a diameter of less than $5/16$ " resulted in an undercoupled cavity. Although data was taken with both undercoupled and overcoupled cavities all of the results reported upon were taken with the undercoupled cavity. The cavity was assembled with silver solder in an atmosphere of hydrogen to prevent excessive oxidation. When oxidation did occur the inside of the guide was polished with a fine grade of carborundum on a wooden swab and washed with a 10% solution of nitric acid.

b. Mounting of Samples

Three methods of mounting the samples were used. If the sample was large enough to cover the end of the guide - this was true of the plated samples and the rolled poly-

crystalline samples - it was soldered directly to the end of the cavity using the hydrogen atmosphere to prevent oxidation. Nickel samples were soldered with pure lead and clamped lightly to keep them fixed in place near the Curie temperature (352°C) where the lead held only due to surface tension. Iron samples were silver soldered.

In order to make the anisotropy measurements the crystals had to be rotated about an perpendicular to the face of the sample. This was accomplished as follows (Figure 6). The bottom of the cavity was closed with a brass block in which a conical hole of 8° taper was bored in such a manner that the small end had a diameter of .400", the nominal inside width of the X-band guide. The sample, soldered with Wood's metal on a matched conical cylinder, was pressed into the end plate and tightly clamped. This made a quite reproducible contact and lent itself readily to the anisotropy measurements. In order to measure the angle a protractor was soldered on the conical cylinder and a small pointer was mounted on the end plate. This device was capable of 2° reproducibility, sufficiently accurate for the data which was taken.

The temperature dependence data on the single crystals was taken as follows. A brass plate large enough to cover the end of the cavity was bored with a cylindrical recess .005" shallower than the thickness of the sample and with the same diameter as the sample. The sample was then soldered into the recess, mechanically polished until the

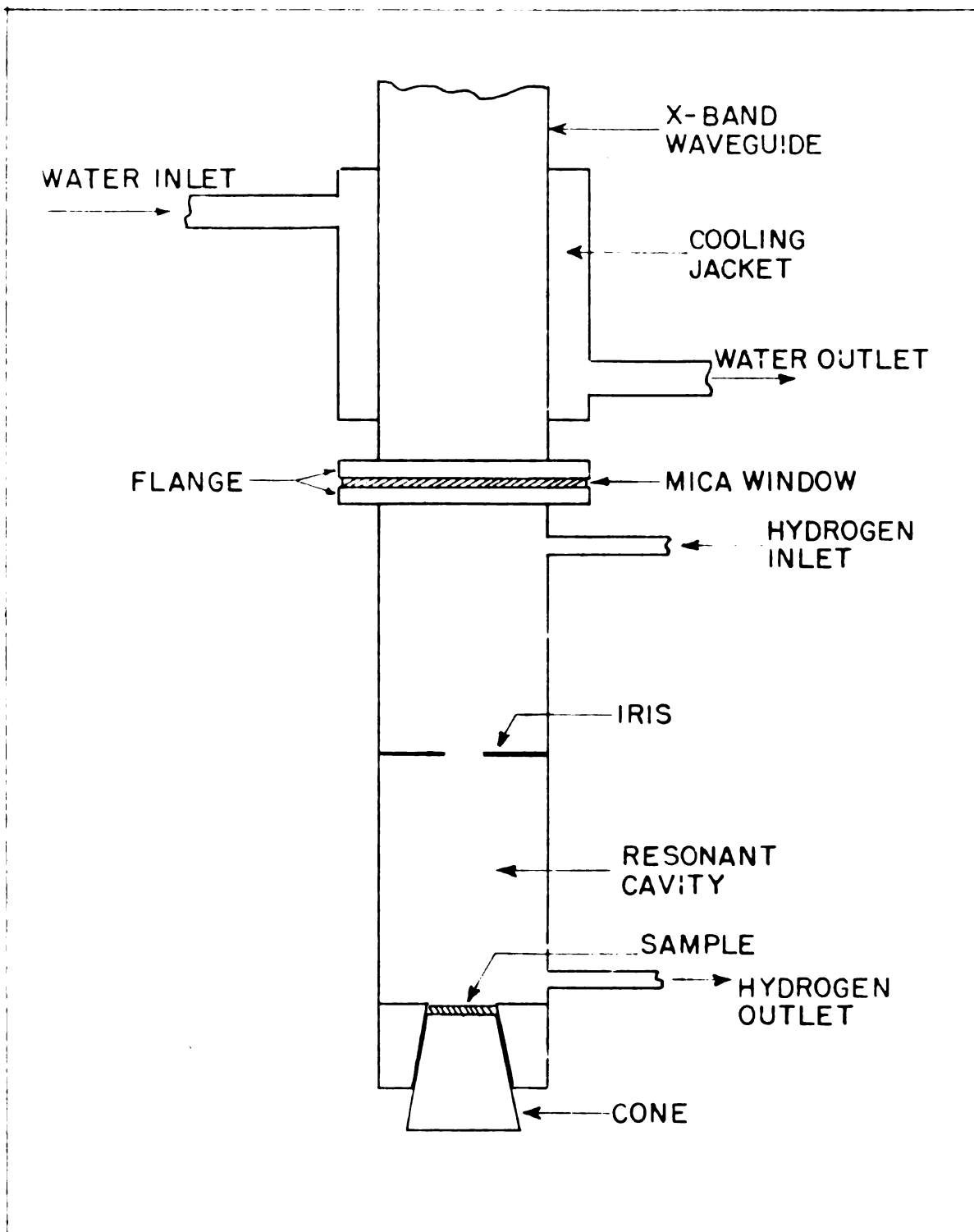


Figure 6. Cavity assembly as used in anisotropy measurements.

sample and plate were flush, electropolished and then the plate was soldered to the guide.

In addition to these methods of mounting, some comparison data was taken with samples clamped against windows in the side wall of the cavity. This data showed considerable variation due to non-reproducibility of contact. Insertion of a thin mica window as suggested by Kip and Arnold only served to decrease the signal strength without adding to the reproducibility.

c. Heating the Sample

The heating coil consisted of 9 ohms of .112" x .005" Nichrome ribbon wound on the cavity in a non inductive manner and operated on A. C. from a Variac. It was wound on a base of asbestos paper and held rigid by a thin layer of potters clay. An insulating layer of glass wool was wrapped on the clay and this in turn held in place with a layer of asbestos applied wet and baked dry. The oven was capable of temperatures up to 800°C with a power input of 500 watts. The temperature was measured with a calibrated Chromel-Alumel thermocouple inserted in the cavity end plate in such a manner that it read the temperature of the block immediately adjacent to the sample. It was checked with a thermocouple mounted in place of the sample to an accuracy of 2°C from room temperature to 600°C. In some cases there were larger thermal lags at higher temp-

eratures but these could always be checked by the fact that no ferromagnetic resonance absorption should be observed above the known Curie temperature. If there was appreciable absorption above this temperature, the data was discarded.

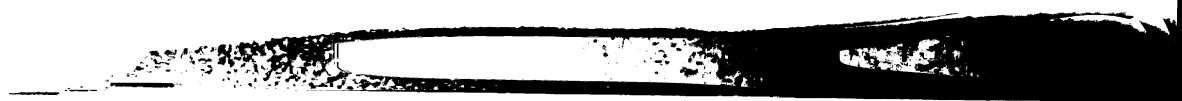
The output of the thermocouple was read on a Leeds and Northrup type K potentiometer. Oxidation of the samples at high temperatures was prevented by passing dried hydrogen gas through the section of the guide containing the cavity. The gas entered above the cavity and was passed out at the bottom through a 1/16" copper tube, where it was burned.

Immediately above the cavity was a section of guide fitted with a water cooling jacket to insure that the remainder of the microwave system was not heated excessively. The mica window to prevent leakage of the hydrogen was mounted on the flange below this cooling coil.

d. The Magnet

The magnet was constructed of SAE 1020 low carbon steel in the form of a square box 22" x 22" x 9". The sides of the box, which were 3 1/2" thick, were machined and bolted together with 1/2" bolts. The pole pieces (7" in diameter), which were machined to slip fit holes bored in the box, were threaded and held in place with retaining rings 1" thick. Since the ferromagnetic re-

sonance line is very wide no special treatment of pole faces to insure a very homogeneous field was undertaken. The copper used was .072" square formvar insulated wire which was wound on four copper bobbins. The bobbins were made of 3/16 " thick copper sheet and were designed so that the finished spool was 15" in diameter and 1 3/4" thick, each with a resistance of approximately 5 ohms. The coils could be connected in series or parallel as required by the power source which in this case was a bank of 12 marine batteries of 300 ampere hour capacity. In spite of the formvar insulation it was found necessary to insulate the wire from the bobbin with a layer of .010" asbestos paper. After winding, the coils were dipped in formvar and wrapped in linen. The magnet was controlled with a potentiometer consisting of a water cooled rheostat capable of carrying 18 amperes, while the magnet current was read on a Westinghouse Type Px-4 meter to an accuracy of about 25 milliamperes in the range 0-5 amperes. In this range the field-current relationship was linear.(Figure 7) The hysteresis of the magnet was approximately 65 gauss and therefore care was taken to read all points in an increasing current. With a pole piece separation of 1 1/4" the magnet was capable of fields of 12,000 oersteds at a current of 18 amperes. The calibration curve was determined with a Sensitive Research Company model F. M. fluxmeter and was calibrated at several points with a proton-resonance signal.



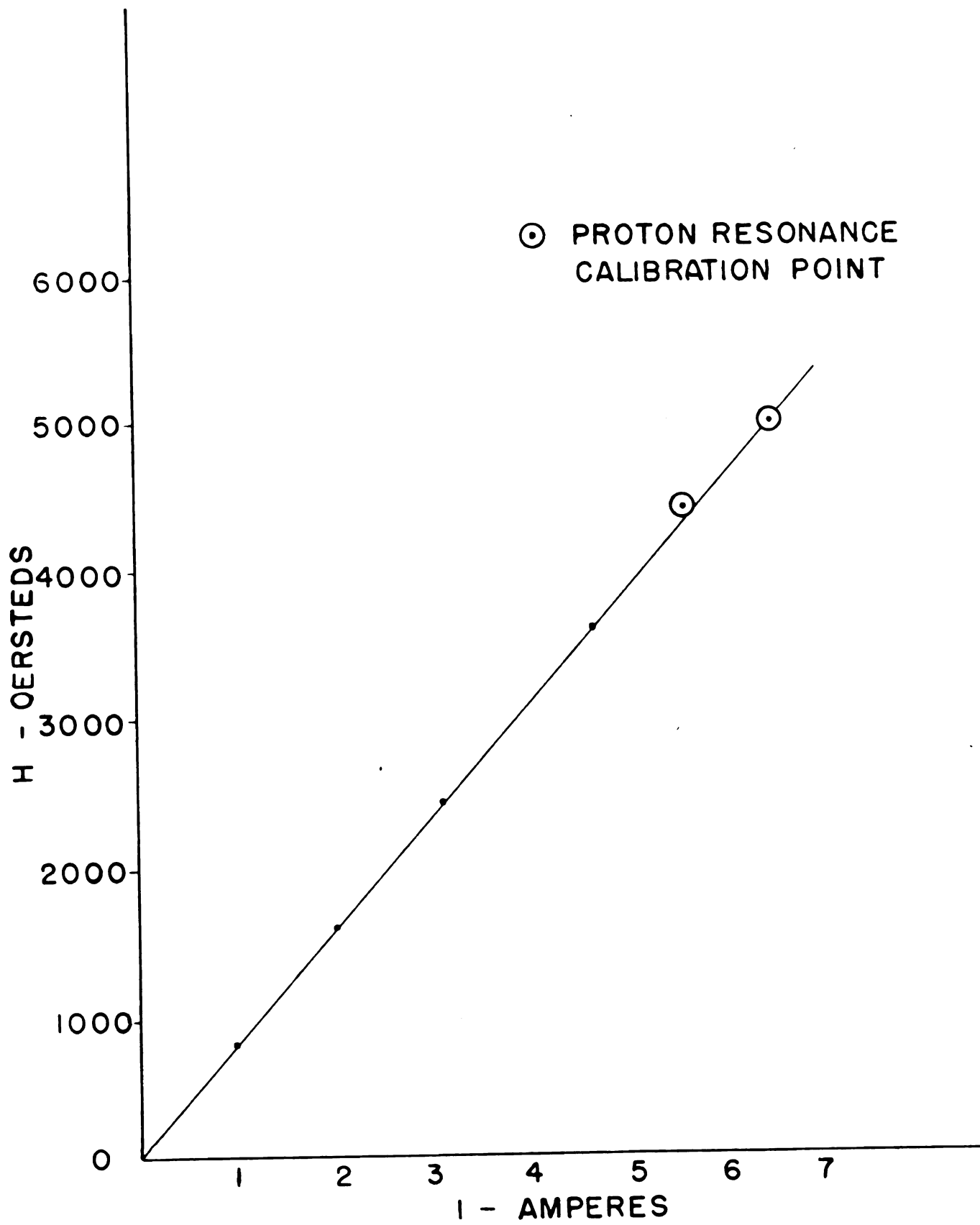
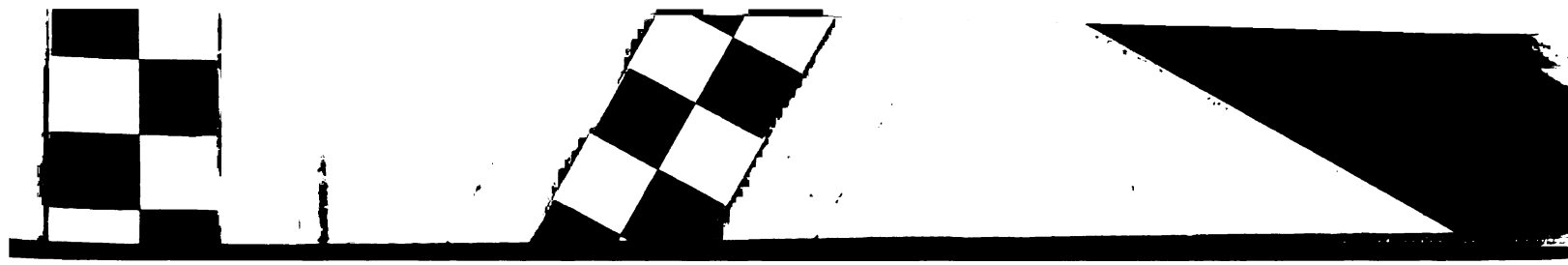


FIG. 7 MAGNET CALIBRATION CURVE

PROTON RESONANCE
CALORIMETER

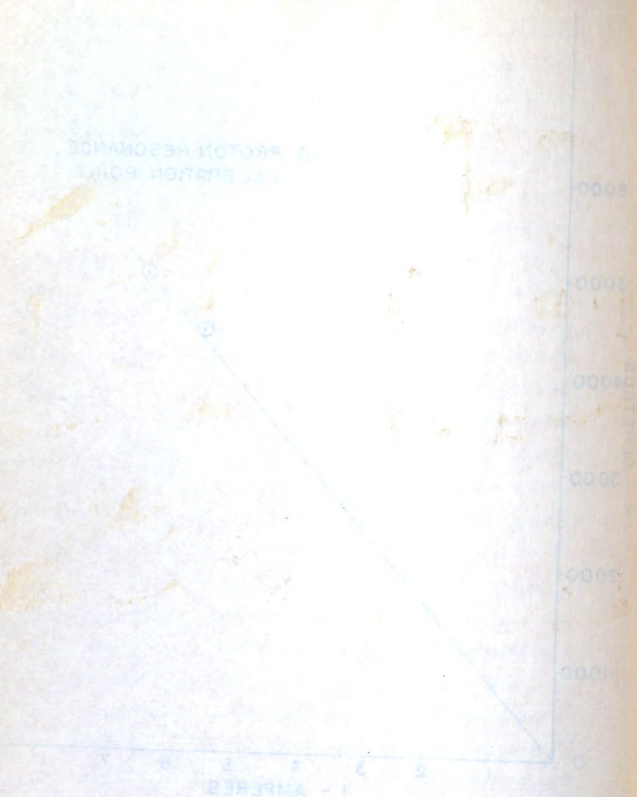


FIG. 1. MAGNET CALORIMETER

e. Preparation of Samples

Samples of three types were used:

1. Electroplated
2. Rolled polycrystalline
3. Single crystal

1. The nickel samples were plated from a commercial bright nickel (Udylite) which was spectroscopically analyzed to show a small amount of cobalt (probably contamination acquired in the laboratory). Samples of a 1% Co-Ni alloy and a 18% Co-Ni alloy were also plated. A typical sample was .001" thick plated on a brass disk. A dull nickel plate was also tried, but this was not successful even after electropolishing.

2. The rolled samples were of two types, a soft temper commercial type A nickel .004" thick, and a 3% Silicon iron oriented alloy .015" thick. These samples were electropolished before use.

3. The single crystal samples came in the form of rods of Armco iron and commercially pure Ni $3/8$ " and $1/2$ " in diameter respectively. The iron rods were etched and crudely oriented visually by means of light reflection from the crystallographic planes; then oriented more accurately by back reflection x-ray methods. The crystals were then cut, on a wet carborundum cut off wheel, into slabs .060" thick, polished and reetched until they were

2. Preparation of samples

Samples of 2 mm diam were used:

1. Pure nickel

2. 10% Ni-90% Cu alloy

3. 10% Ni-90% Cu alloy

1. The 10% Ni-90% Cu alloy was prepared from a commercial

bright nickel (99.99% Ni) and copper (99.99% Cu).

samples to make a small amount of sample (probably con-

tamination resulting in the formation of a thin layer of a

10-20 Ni alloy and a 10-20 Cu alloy were also made.

A typical sample of 10-20 Ni alloy was in a brass disk.

A dull nickel 10-20 Ni alloy disk was also made and was not

examined even after the 10-20 Ni alloy.

2. The 10% Ni-90% Cu alloy of two types, a soft

temper commercial grade (99.99% Ni) and a 99.99%

99.99% Ni-90% Cu alloy. These samples

were electroplated onto the

3. The 10% Ni-90% Cu alloy was in the form of

rods of 2 mm diam and commercially pure 10-20% and 10-20%

in diameter respectively. The 10-20% rods were etched and

carefully oriented (usually by means of light reflection

from the crystallographic faces) then oriented more ac-

curely by back reflection X-ray method. The crystals

were then cut, on a lathe or by hand, into

shape .050" thick, polished and rechecked until they were

thin enough for transmission laue patterns to be taken. After accurate orientation (to less than $1/2^\circ$ in the best cases) they were mounted on a brass rod with Woods metal and made oblate spheroids with file and emery paper while turning in a lathe. The samples were then re-etched, one surface electropolished and were then removed from the rod ready for use.


The preparation of the nickel samples was the same as the iron except that it was not possible to find an etching reagent to bring out the crystallographic planes and therefore even the rough orientation was done by x-ray methods.

The x-ray source was a North American Phillips unit with a Molybdenum target. The cameras which were used were built so that the single crystal rods could be taken off of the camera and put into the saw mounted on a universal head. This was accomplished by use of a holder with two mutually perpendicular axes of rotation on which the rod was mounted in a split collet and held in place with set screws. The base of the holder was mounted on a camera consisting of a film holder and a vertical plate. When the sample was oriented and ready for cutting, the sample holder was taken off of the vertical plate and clamped in the vise. In this way it was not necessary to remove the rod in order to cut it. The orientation of the sample camera was checked by transmission and back reflection Laue patterns of freshly cleaved rock salt.

This camera was found in the water to be taken. After several hours this film was taken in the boat (camera) they were mounted in a small box with metal and made out of glass with film and a very narrow white turning in a circle. The film was then removed, one surface of the film was then removed from the box and ready for use.

The camera film of the night camera was the same as the film exposed but it was not possible to find an existing camera to which the photographic plates and therefore even the film examination was done by x-ray methods.

The camera was a home American Bellini unit with a 16mm lens. The camera which were used were built so that the film exposed could be taken off of the camera and put into the saw mounted on a universal head. The film was exposed by use of a holder which two mutually perpendicular axes of rotation on which the rod was mounted in a small circle and held in place with set screws. The base of the holder was mounted on a camera consisting of a film holder and a vertical plate. When the camera was oriented and ready for cutting, the sample holder was taken off of the vertical plate and clamped in the view. In this way it was not necessary to remove the rod in order to use it. The orientation of the sample camera was checked by transmission and back reflection lane patterns of freshly cleaved rock salt.



f. Electrolytic Polishing

The first work on the electrolytic polishing of copper was done in 1938 by Jacquet¹⁸. Elmore¹⁹ extended both the theory and technique to iron and cobalt. Although it is used extensively in large scale industrial polishing, the technique as applied to small samples is not well known and therefore will be described here in some detail. The process involves the electrolytic removal of the anode material in which the rate of removal is determined by the layer of dissolved material surrounding the anode, rather than the anode potential itself.

Figure 8 shows the experimental apparatus. The cell consists of a wide mouth jar with the bottom cut off. A hole is bored in the top and the sample, mounted on a brass rod, is fixed in the hole with red wax, first insuring that the brass is protected from the electrolytic action by a thin coat of lacquer. The cathode is a brass ring which fits into the large part of the jar. The sample is mounted horizontally so that the dissolved iron will not flow away from the surface.

The actual currents and voltages observed vary with anode and cathode material and area as well as electrolyte concentration, therefore the numbers are given only for a typical sample of armco iron in the form of a disc .302" in diameter.

The first work on the electrolytic refining of copper was done in 1855 by James W. Elmore,¹² who extended both the theory and technique of iron and cobalt. Although it is now extensively used in large scale industrial refining, the technique as applied to small samples is not well known and therefore will be described here in some detail. The process involves the electrolytic removal of the anode material in which the rate of removal is determined by the type of dissolved material surrounding the anode, rather than the anode potential itself. Figure 3 shows the experimental apparatus. The cell consists of a wide mouth jar with the bottom cut off. A hole is bored in the top and the sample, mounted on a brass rod, is fitted in the hole with red wax, fitted in-
 ensuring that the brass is protected from the electrolytic action by a thin coat of lacquer. The cathode is a brass ring which fits into the large end of the jar. The sample is mounted horizontally so that the dissolved ions will not flow away from the surface. The actual currents and voltages observed vary with anode and cathode material and area as well as electrolyte concentration, therefore the numbers are given only for a typical sample of brass iron in the form of a disc .302" in diameter.

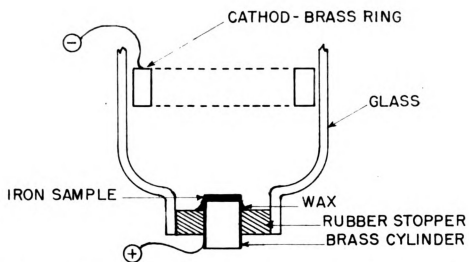
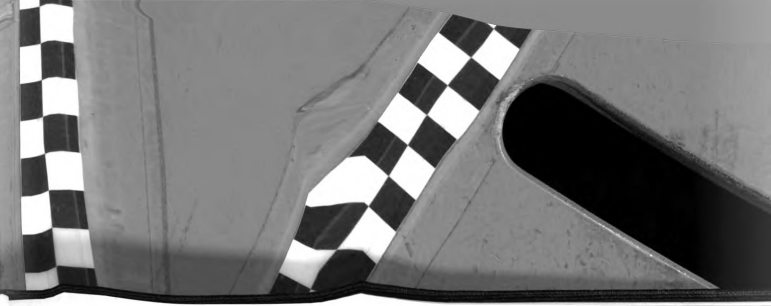


Figure 8. Experimental apparatus for electrolytic polishing of small iron samples

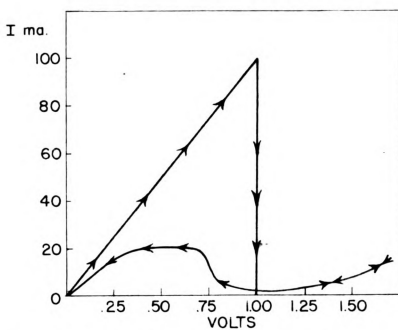
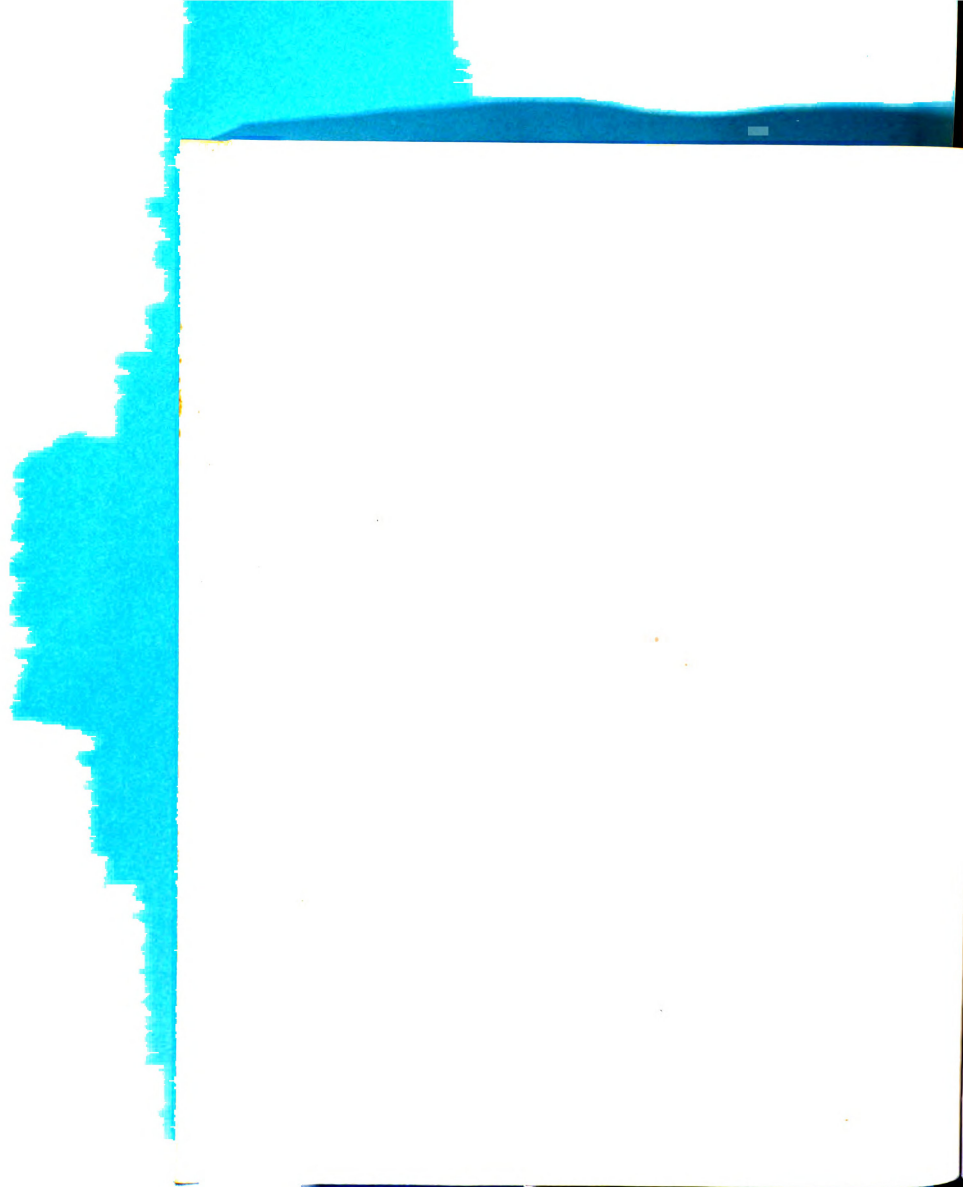
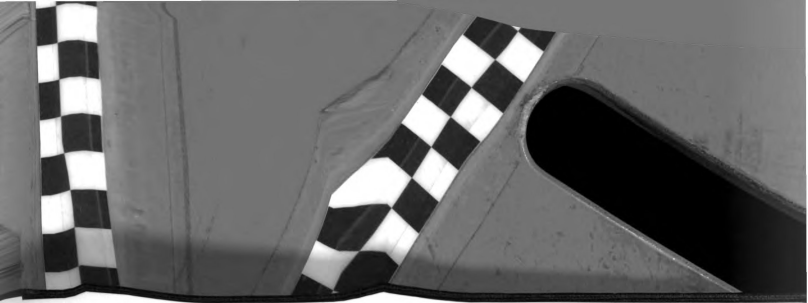


Figure 9. Electrical characteristics of the polishing cell





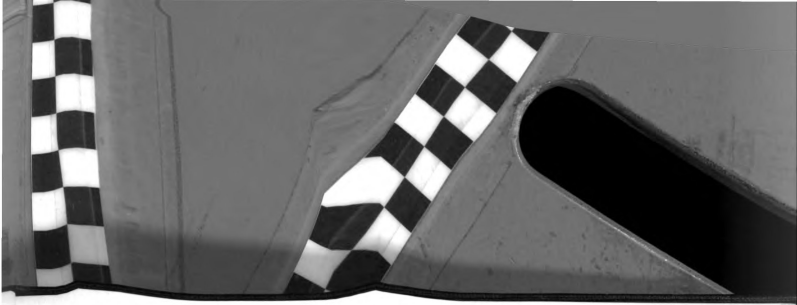
For iron the electrolyte is orthophosphoric acid of specific gravity 1.32 in which a dummy iron cathode has been allowed to dissolve for 15 or 20 minutes. This apparently insures a certain amount of iron in the bath.

When the cell is first connected and the voltage increased from 0 to 1 volt the current increases linearly to about 100 milliamperes (Figure 9). If the voltage is increased further the current will continue to increase but much more slowly. If the voltage is now decreased to approximately .6 volt the current increases sharply to 18 milliamperes after which a further decrease in voltage has but slight effect on the current. This plateau is approximately .25 volts wide after which the current drops to zero at zero volts. The best polishing is obtained when the cell is operated on this plateau in the voltage-current curve. Initially there may be slight pitting but this will give way to a high gloss which may have microscopic ripples or waves.

According to Elmore the current density must be quite uniform at the anode and the cell voltage kept within the narrow range. The electrolyte must contain some dissolved iron so that the anode is not too readily etched by the acid. The straight portion occurs before polarization at the anode takes place and is essentially the IR drop through the cell. The important factor is the concentration layer of dissolved iron at the anode which serves two purposes: 1) it introduces an opposing emf. and 2)

For from the electrolyte is out of the electrolyte cell of
 specific gravity 1.12 in which a dummy iron cathode has
 been allowed to dissolve for 15 or 20 minutes. This has
 partially immersed a certain amount of iron in the bath.
 When the cell is first connected and the voltage in-
 creased from 0 to 1 volt the current increases linearly
 to about 100 milliamperes (Figure 3). If the voltage is
 increased further the current will continue to increase
 but much more slowly. If the voltage is now decreased to
 approximately 0.5 volt the current increases sharply to
 10 milliamperes after which a further decrease in voltage
 has but little effect on the current. This plateau is
 approximately 10 volts wide after which the current drops
 to zero at zero volts. The best voltages is obtained
 when the cell is operated on this plateau in the voltage-
 current curve. Initially there may be slight etching but
 this will give way to a high gloss which may have micro-
 scopic ripples or waves.

According to Brown the current density must be quite
 uniform at the anode and the cell voltage kept within the
 narrow range. The electrolyte must contain some dissolved
 iron so that the anode is not too readily etched by the
 acid. The etching portion occurs before polarization at
 the anode takes place and is essentially the IR drop
 through the cell. The important factor in the concentra-
 tion layer of dissolved iron at the anode which serves
 two purposes: 1) it introduces an opposing emf. and 2)



when this back emf. has reached a definite value the layer serves to limit the current through the cell. The layer is produced by slow diffusion of newly dissolved anode material into the main body of the electrolyte.

The polishing occurs when the rate of solution of iron is limited by the concentration gradient existing at the anode. Since this gradient is greatest near portions which project, these portions will dissolve more rapidly. No etching takes place because only the concentration layer determines the rate at which the anode dissolves and not the anode material itself.

The technique used on nickel samples was that described by Bloembergen⁶. This method used 10% chromic acid and 90% orthophosphoric acid used at 90°C and with high current densities (20 amperes per square centimeter). This does not appear to be a true electropolishing method but rather an electrolytic etching process. Although the surfaces of the nickel became highly polished it appears that they were still somewhat strained as shown by the results of domain investigations.

g. Domain Structure

Since all of the factors which determine the line width are not known and since the skin depth for 3 centimeter microwaves is approximately 10^{-5} centimeters, every effort was made to obtain surfaces essentially free of strain. In order to do this the samples were cut to orientation on a wet wheel .025" thick, were then polished and

when this peak end, has reached a definite value the layer
nerves to limit the current to a set value. The layer
is produced by slow diffusion of metal dissolved under
material into the main body of the electrode.

The electrode reaction and the rate of solution of
iron is limited by the concentration gradient existing at
the anode. Since this is a very slow process near portions
which project, the concentration gradient is more readily
No staining is observed when the concentration
layer determines the rate of solution of the anode dissolves
and not the rate of diffusion.

The electrode reaction is a function of the rate of
oxidation by the electrode. This method used for anodic
acid and 10% and 20% and 30% and 40% and 50% and 60% and 70% and 80% and 90% and 100% and with
high current densities. (It remains for future consideration.)
This does not appear to be a true electrochemical method
but rather an electrochemical process. Although
the number of the nickel atoms highly polished is
apparent that they were still covered as shown
by the results of certain investigations.

E. Domain Structure

Since all of the factors which determine the line
width are not known and since the line width for 2 centi-
meter microwaves is approximately 10^{-5} centimeters, every
effort was made to obtain surfaces essentially free of
strain. In order to do this the samples were cut to obtain
action on a wet wheel, 0.02" thick, were then polished and



etched alternately until at least .015" was removed from each face. The samples were then electrolytically polished or etched until very shiny surfaces (surfaces of high specular reflection) were obtained. In order to insure a minimum of strains the surfaces were examined for domains using the colloidal particle technique of McKeehan and Elmore²⁰. It is to be noted that later writers were not as specific in their directions for the preparation of the colloidal solution as Elmore and that best results are obtained by following his original directions. If the strains are not removed in the etching and polishing process, a domain pattern characteristic of strained surfaces is observed. If the strains are removed, domain patterns characteristic of the particular crystallographic orientation are observed. In the best cases the armco iron showed regions of strain alternating with unstrained regions. The domain structure on the nickel was very difficult to observe and in most cases the surface showed an anomalous pattern unlike either the strained or unstrained. In these cases the optimum condition of the surface was determined by taking room temperature curves with successively increasing amounts of electropolishing.

V. ANALYSIS OF DATA

The actual evaluation of the quantities A and B given in Equation 3-7 involves making two completely different types of measurements for each resonance curve and a calculation of Q_0 . Since the calculated values of Q_0 do not compare favorably with experimentally determined values, it is desirable to eliminate the evaluation of

A and B. Rewriting 3-7
$$A\sqrt{\mu'} + B = \frac{\alpha + p^{1/2}}{\alpha - p^{1/2}} \quad 3-7$$

Let μ'_{res} be the value of μ' at ferromagnetic resonance, then

$$A\sqrt{\mu'_{res}} + B = \frac{\alpha + p_{res}^{1/2}}{\alpha - p_{res}^{1/2}} \quad 5-1$$

where p_{res} is the power measured at resonance. Inspection of Equation 2-15 shows that at large fields μ' approaches 1, hence

$$A + B = \frac{\alpha + p_{\infty}^{1/2}}{\alpha - p_{\infty}^{1/2}} \quad 5-2$$

where p_{∞} is the power measured at large fields. Combining 3-7, 5-1, 5-2 we obtain

$$R = \frac{\sqrt{\mu'} - 1}{\sqrt{\mu'_{res}} - 1} = \left(\frac{\alpha - p_{res}^{1/2}}{\alpha - p^{1/2}} \right) \left(\frac{p^{1/2} - p_{\infty}^{1/2}}{p_{res}^{1/2} - p_{\infty}^{1/2}} \right) \quad 5-3$$

Since the ratio R involves only quantities which can be directly measured, it can easily be determined as a function of H_0 . It remains to be shown that a knowledge of R as a function of H_0 is sufficient to determine $1/T_2$. Two

methods have been developed to show this, the first method given is exact, the second is approximate.

Rewriting Equations 2-15

$$\mu_1 = \frac{4\pi\gamma^2 M_0 [H_0 + (N_y' - N_z') M_0] (\omega_0^2 - \omega^2)}{(\omega_0^2 - \omega^2)^2 + 4\omega^2 T_2^2} + 1$$

$$\mu_2 = \frac{4\pi\gamma^2 M_0 [H_0 + (N_y' - N_z') M_0] 2\omega/T_2}{(\omega_0^2 - \omega^2)^2 + (2\omega/T_2)^2}$$

Let $H_{0/2}^+$ and $H_{0/2}^-$ be two values of H_0 such that

$$\omega_0^2 - \omega^2 = 2\omega/T_2 \quad \text{for } H_0 = H_{0/2}^+ \quad 5-4a$$

$$\omega_0^2 - \omega^2 = -2\omega/T_2 \quad \text{for } H_0 = H_{0/2}^- \quad 5-4b$$

Thus from Equation 2-16 it appears that $H_{0/2}^+$ and $H_{0/2}^-$ must be solutions of

$$H_{0/2}^2 - H_{0_{res}}^2 + 2\eta (H_{0/2} - H_{0_{res}}) \pm \delta = 0 \quad 5-5$$

where $2\eta = (N_x' + N_y' - 2N_z') M_0 \quad 5-6$

$$\delta = \frac{2\omega}{\gamma^2 T_2^2} \quad 5-7$$

and N' includes both anisotropy and shape demagnetization factors. Hence

$$H_{0/2}^+ + \eta = [(H_{0_{res}} + \eta)^2 + \delta]^{1/2} \quad 5-8a$$

$$H_{0/2}^- + \eta = [(H_{0_{res}} + \eta)^2 - \delta]^{1/2} \quad 5-8b$$

thus

$$\frac{1}{2} [(H_{0/2}^+ + \eta)^2 + (H_{0/2}^- + \eta)^2] = (H_{0_{res}} + \eta) \quad 5-9$$

and

$$\frac{1}{2} [(H_{0/2}^+ + \eta)^2 - (H_{0/2}^- + \eta)^2] = \delta = \frac{2\omega}{\gamma^2 T_2^2} \quad 5-10$$

methods have been developed to show that the time

method given is correct, the second is approximate.

Reverting to the 2-10

$\frac{1}{2} = \frac{1}{2}$

$\frac{1}{2} = \frac{1}{2}$

Let $\frac{1}{2}$ and $\frac{1}{2}$ be the values of $\frac{1}{2}$ such that

2-10

2-10

Thus from 2-10 it is seen that $\frac{1}{2}$ and $\frac{1}{2}$

must be satisfied if

2-10

where

2-10

2-10

and $\frac{1}{2}$ includes both angles $\frac{1}{2}$ and where demonstration

factor. Hence

2-10

2-10

Thus

2-10

and

2-10

Thus it is seen that if $H_{o\frac{1}{2}}^+$ and $H_{o\frac{1}{2}}^-$ can be determined, $1/T_2$ can be obtained.

Let R^+ and R^- be the values of $R(H_o)$ corresponding to $H_{o\frac{1}{2}}^+$ and $H_{o\frac{1}{2}}^-$ respectively. Combining Equations 2-15, 5-3, 5-4, 5-6, 5-7, we find

$$R^+ = \frac{[\sqrt{(H_{o\frac{1}{2}}^+ + \lambda)^2 + (H_{o\frac{1}{2}}^+ + \lambda + \beta)^2} + (H_{o\frac{1}{2}}^+ + \lambda)]^{\frac{1}{2}} - \beta^{\frac{1}{2}}}{[\sqrt{4(H_{o\text{res}} + \lambda)^2 + \beta^2} + 2(H_{o\text{res}} + \lambda)]^{\frac{1}{2}} - \beta^{\frac{1}{2}}} \quad 5-11a$$

$$R^- = \frac{[\sqrt{(H_{o\frac{1}{2}}^- + \lambda)^2 + (H_{o\frac{1}{2}}^- + \lambda + \beta)^2} + (H_{o\frac{1}{2}}^- + \lambda)]^{\frac{1}{2}} - \beta^{\frac{1}{2}}}{[\sqrt{4(H_{o\text{res}} + \lambda)^2 + \beta^2} + 2(H_{o\text{res}} + \lambda)]^{\frac{1}{2}} - \beta^{\frac{1}{2}}} \quad 5-11b$$

where

$$\beta = \frac{2}{4\pi M_o} \left\{ (H_{o\frac{1}{2}}^+ + \eta)^2 - (H_{o\text{res}} + \eta)^2 \right\} \quad 5-12a$$

or

$$\beta = \frac{2}{4\pi M_o} \left\{ (H_{o\text{res}} + \eta)^2 - (H_{o\frac{1}{2}}^- + \eta)^2 \right\} \quad 5-12b$$

and

$$\lambda = (N_y' - N_z') M_o \quad 5-13$$

To determine $1/T_2$ from the data, a curve of $R(H_o)$ against H_o is plotted as shown in Figure 10. Then R^+ and R^- are plotted on the same graph. The intersection of R^+ and R^- with R give the values of $H_{o\frac{1}{2}}^+$ and $H_{o\frac{1}{2}}^-$ appropriate to the experiment. $1/T_2$ is then found from Equation 5-10.

The preceding method involves some rather tedious calculations and therefore the following approximate method is given. Under most conditions its accuracy is within the limits imposed by the fundamental data. Let us define line width as $\Delta H = H_{o\frac{1}{2}}^+ - H_{o\frac{1}{2}}^-$ 5-14

Thus it is seen that $1/\lambda$ and λ can be determined.
 $1/\lambda$ can be obtained.

Let R and R' be the values of $R(\lambda_0)$ corresponding
 to λ_0 and λ'_0 respectively. Combining Equations 2-12,
 2-13, 2-14, 2-15, we find

$$R' - R = \frac{1}{\lambda_0^2} \left(\frac{1}{\lambda_0} - \frac{1}{\lambda'_0} \right) \quad 2-16$$

$$R' - R = \frac{1}{\lambda_0^2} \left(\frac{1}{\lambda_0} - \frac{1}{\lambda'_0} \right) \quad 2-17$$

$$\text{where} \quad 2-18$$

$$\text{or} \quad 2-19$$

and
 2-20
 To determine $1/\lambda$ from the data curve of $R(\lambda_0)$ against
 λ_0 is plotted as shown in Figure 10. Then R and R' are
 plotted on the same graph. The intersection of R and R'
 with R give the values of λ_0 and λ'_0 appropriate to
 the experiment. $1/\lambda_0$ is then found from Equation 2-10.
 The preceding method involves some rather tedious
 calculations and therefore the following approximate
 method is given. Under most conditions the accuracy is
 within the limits imposed by the fundamental data. Let
 as define line width as

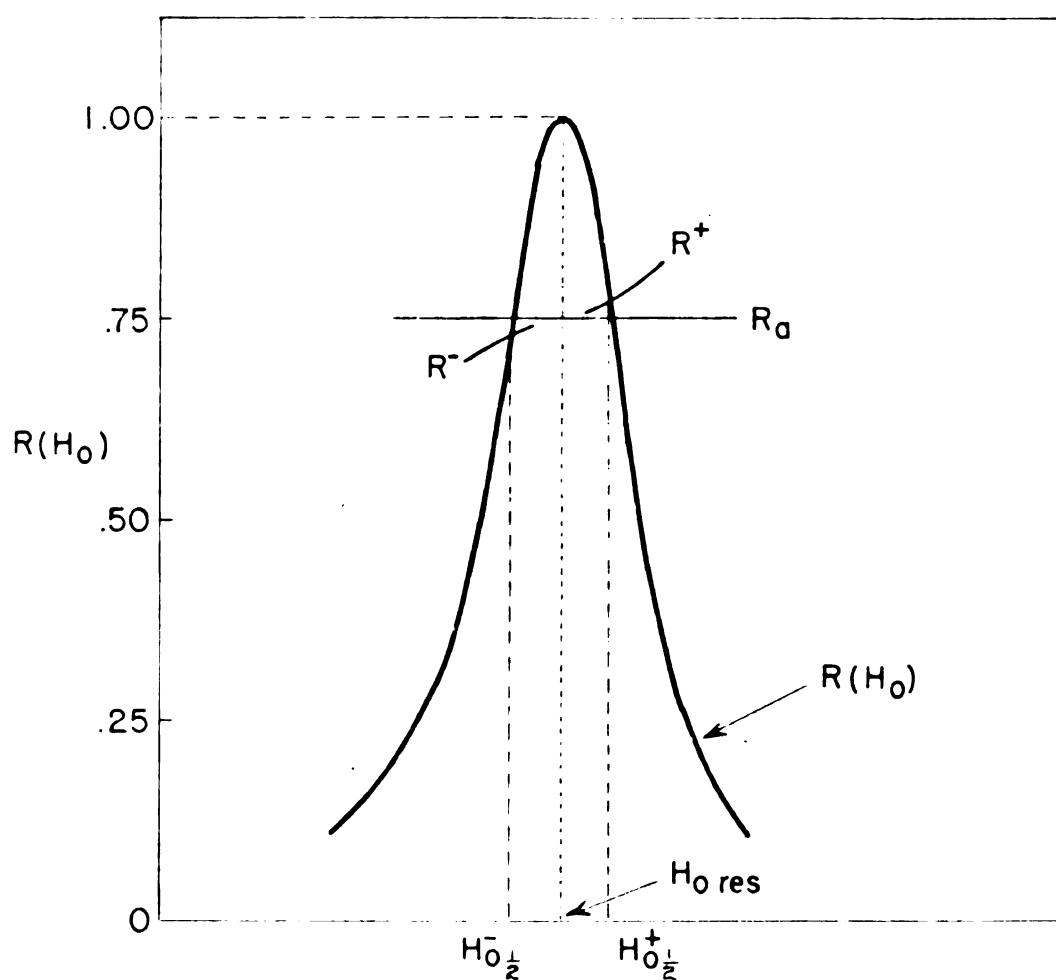
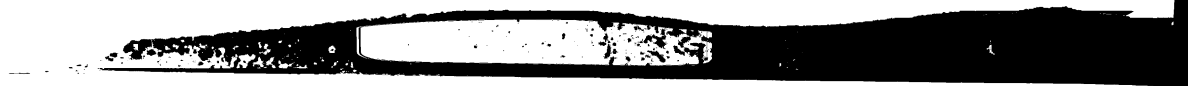


Figure 10. The method of determining H_0^+ and H_0^- from the experimental curve $R(H)$ and the theoretical curve R^+ and R^- .



Expanding the right hand side of Equations 5-3a and 5-8b by the binomial theorem one finds

$$\Delta H = \frac{\delta}{H_{ores} + \eta} \left\{ 1 + \frac{1}{\delta} \left(\frac{\delta}{(H_{ores} + \eta)^2} \right)^2 + \dots \right\} \quad 5-15$$

Order of magnitude estimates of the quantities involved show that only the first term need be considered. Hence

$$\delta \approx (H_{ores} + \eta) \Delta H \quad 5-16$$

and

$$\frac{1}{T_2} \approx \frac{\delta^2}{2w} \delta = \frac{\delta^2}{2w} (H_{ores} + \eta) \Delta H \quad 5-17$$

Thus we can determine $1/T_2$ by measuring the resonance field and the line width. ΔH may be obtained from a plot of $R(H_0)$ as follows. Let $\mu_{2/2}^+$ and $\mu_{2/2}^-$ be the values of $\mu_{2/2}$ at H_0 equal to $H_{0/2}^+$ and $H_{0/2}^-$ respectively. Then from Equations 2-15, 5-4a, and 5-4b

$$\mu_{2/2}^+ \approx \mu_{2/2}^- \approx \frac{1}{2} \mu_{2res} \quad 5-18$$

$$\mu_{2/2}^+ \approx \mu_{2/2}^+ + 1 \approx \frac{1}{2} \mu_{2res}^+ + 1 \quad 5-19$$

We shall therefore drop the superscripts $+$ and $-$. Inserting these results in Equation 2-9a, we obtain

$$\mu'_{1/2} \approx \left[\left(1 + \frac{1}{2} \mu_{2res} \right)^2 + \left(\frac{\mu_{2res}}{2} \right)^2 \right]^{1/2} + \frac{\mu_{2res}}{2} \quad 5-20$$

Similarly

$$\mu'_{res} \approx \left[1 + (\mu_{2res})^2 \right]^{1/2} + \mu_{2res} \quad 5-21$$

We insert these approximate expressions for $\mu'_{1/2}$ and μ'_{res}

Expanding the above and using the binomial theorem one finds

2-15

Order of magnitude estimates of the various involved show that only the first term need be considered. Hence

2-16

and

2-17

Thus we can determine ΔT by measuring the resonance field and the line width. We obtain from a plot of $R(H_0)$ as follows. Let and be the values of H_0 at H_0 equal to and respectively. Then from Equations 2-15, 2-16, and 2-17

2-18

2-19

We shall therefore take the approximation and . In carrying these results in Equation 2-20, we obtain

2-20

Similarly

2-21

We insert these approximate expressions for and

in Equation 5-3 and obtain a ratio

$$R_a = \frac{[(1 + \frac{1}{2} \mu_{2,rev})^2 + (\frac{\mu_{2,rev}}{2})^2 + \frac{\mu_{2,rev}}{2}]^{\frac{1}{2}} - 1}{[(1 + \mu_{2,rev}^2)^{\frac{1}{2}} + \mu_{2,rev}]^{\frac{1}{2}}} \quad 5-22$$

The quantity R_a should approximate R^+ and R^- at their intersections with $R(H_0)$, and therefore the intersections of R_a with $R(H_0)$ give approximate values of $H_{0, \frac{1}{2}}^+$ and $H_{0, \frac{1}{2}}^-$. We note that R_a is a rather slowly varying function of $\mu_{2,rev}$ (Table I) and therefore expect that the actual value of

TABLE I
VALUES OF R_a FOR VARIOUS VALUES OF $\mu_{2,rev}$

| $\mu_{2,rev}$ | R_a |
|---------------|-------|
| 45 | .756 |
| 40 | .755 |
| 35 | .754 |
| 30 | .753 |
| 25 | .751 |
| 20 | .749 |
| 15 | .747 |
| 10 | .742 |
| 5 | .738 |

$1/T_2$ is relatively insensitive to the value of $\mu_{2,rev}$ used. Of course it is necessary to have a value of $\mu_{2,rev}$ with which to obtain R_a . From Equations 2-15 and 5-17 we have

$$\mu_{2,rev} \approx \frac{4\pi M_0 (H_{0,rev} + \lambda)}{\Delta H (H_{0,rev} + \eta)} \quad 5-23$$

In Equation 2-1 and obtain a result

2-22

The quantity R_0 is a constant and at their intersection with R_0 , and therefore the intersection of R_0 with R_0 has approximate values of 1 and 1. We note that R_0 is a relatively slowly varying function of R_0 (Table I) and therefore expect that the actual value of

TABLE I

VALUES OF R_0 FOR VARIOUS VALUES OF R_0

| | |
|------|-------|
| 1.0 | 1.000 |
| 1.2 | 1.008 |
| 1.4 | 1.016 |
| 1.6 | 1.024 |
| 1.8 | 1.032 |
| 2.0 | 1.040 |
| 2.2 | 1.048 |
| 2.4 | 1.056 |
| 2.6 | 1.064 |
| 2.8 | 1.072 |
| 3.0 | 1.080 |
| 3.2 | 1.088 |
| 3.4 | 1.096 |
| 3.6 | 1.104 |
| 3.8 | 1.112 |
| 4.0 | 1.120 |
| 4.2 | 1.128 |
| 4.4 | 1.136 |
| 4.6 | 1.144 |
| 4.8 | 1.152 |
| 5.0 | 1.160 |
| 5.2 | 1.168 |
| 5.4 | 1.176 |
| 5.6 | 1.184 |
| 5.8 | 1.192 |
| 6.0 | 1.200 |
| 6.2 | 1.208 |
| 6.4 | 1.216 |
| 6.6 | 1.224 |
| 6.8 | 1.232 |
| 7.0 | 1.240 |
| 7.2 | 1.248 |
| 7.4 | 1.256 |
| 7.6 | 1.264 |
| 7.8 | 1.272 |
| 8.0 | 1.280 |
| 8.2 | 1.288 |
| 8.4 | 1.296 |
| 8.6 | 1.304 |
| 8.8 | 1.312 |
| 9.0 | 1.320 |
| 9.2 | 1.328 |
| 9.4 | 1.336 |
| 9.6 | 1.344 |
| 9.8 | 1.352 |
| 10.0 | 1.360 |

R_0 is relatively insensitive to the value of R_0 used. Of course it is necessary to have a value of R_0 with which to obtain R_0 . From Equations 2-18 and 2-19 we have

2-23

Thus to find $1/T_2$ one proceeds as follows:

1. The data consists of a plot of p as a function of H_0 with a single value of ρ measured for one point on the curve so that α may be calculated from Equation 3-6a and $R(H_0)$ obtained from Equation 5-3.

2. Assume $R_a \simeq .75$. Draw a line on the plot of $R(H_0)$ at .75 and read off the distance (in oersteds) between the intersection points. This is a first approximation to ΔH .

3. From Equation 5-23 compute an approximate value of μ_{2rev} . From Table I find a second approximation for R_a and then from $R(H_0)$ a second approximation for ΔH .

4. Calculate $1/T_2$ from Equation 5-17.

Generally two approximations are sufficient to give all of the accuracy available in this method. In cases in which $\mu' = 1$ is not a good approximation at the highest fields available one obtains a better approximation as follows. Let H_{0L} be the largest field at which measurements are made. Then μ' at H_{0L} is given approximately by

$$\mu'_L = 1 + \frac{4\pi M_0}{H_{0L}} \left\{ \frac{1}{1 - \frac{H_{0res}(H_{0res} + 4\pi M_0)}{H_{0L}(H_{0L} + 4\pi M_0)}} \right\} \quad 5-24$$

This is inserted in place of unity in the numerator and denominator of Equation 5-3. Equation 5-23 is corrected by replacing unity in the numerator and denominator by μ'_L .

It is obvious that the approximate method depends on several assumptions and it will be worth while here to

Thus to find λ_0 one proceeds as follows:
 1. The first estimate of λ_0 is obtained from
 the solution of R_0 with a single value of λ measured for
 one point on the curve so that λ_0 is calculated from
 Equation 3-1a and R_0 obtained from Equation 3-1.
 2. Assume $\lambda = \lambda_0$. Then a line on the plot of
 $R(\lambda_0)$ at λ_0 and read off the distance (in centimeters)
 between the intersection of λ_0 and the line and the
 location of λ_0 .

3. This distance is used as an approximate
 value of λ_0 . Then λ_0 is used as a second approximation
 for λ_0 and from Equation 3-1a a second approximation for λ_0 .
 4. Repeat steps 1-3 from Equation 3-1a.

Generally the method of successive approximations to give all
 of the necessary results in this method. In cases in
 which λ_0 is not a good approximation of the highest
 fields available one obtains a better approximation as
 follows. Let λ_0 be the largest field at which measure-
 ments are made. Then λ_0 is given approximately by

$$\lambda_0 = \frac{1}{2} \left(\frac{1}{\lambda_0} + \frac{1}{\lambda_0} \right)$$

This is inserted in place of unity in the numerator and
 denominator of Equation 3-1. Equation 3-1a is corrected
 by replacing unity in the numerator and denominator by λ_0 .
 It is obvious that the approximate method depends on
 several assumptions and it will be worth while here to

evaluate these and estimate the error encountered in the evaluation of $1/T_2$ by this method.

Let us consider the assumptions:

1. $\mu' = 1$ at highest fields available. Both the exact and approximate treatments depend on this assumption but we have shown in Equation 5-24 how to eliminate it where it is unwarranted and obtain an exact value.

2. $\mu_{2,1/2} \simeq \frac{1}{2} \mu_{2,rel}$ There are actually several assumptions inherent in this approximation but since it is possible to calculate this without reference to the assumptions it is not necessary to discuss them explicitly. It suffices to say that in the very worse cases this may introduce an error of 15% in $R(H_0)$.

3. $\frac{\delta}{(H_0 + \eta)^2} \ll 1$ Typical calculations on this quantity show that it can never introduce an error of as much as 1%.

Thus far we have assumed that γ^2 is known which is actually not the case. If we examine Equation 2-16 we see that by knowing N_x', N_y', N_z', M_0 , and $\frac{1}{T_2}$, it is possible to calculate γ^2 . Since, of course, $1/T_2$ is not known, it is necessary to approximate γ^2 by neglecting $1/T_2$ in Equation 2-16. If we neglect $1/T_2$ and obtain γ_0^2 then put this into Equation 5-17 to obtain an approximation to $1/T_2$, we can approach γ^2 and $1/T_2$ by successive approximations. For small values of $1/T_2$ these corrections are small and even for the largest values observed the error is less than 10%.

estimate these and estimate the error associated in the

evaluation of $\sqrt{V_2}$ by this method.

Let us consider the assumptions:

1. $\sqrt{V_2}$ is not a function of $\sqrt{V_1}$. Both the

exact and approximate theories depend on this assumption

but we have shown in Equation 2-16 how to eliminate it

where it is unnecessary to obtain an exact value.

2. There are actually several

assumptions involved in this approximation but since it

is possible to estimate this without reference to the

assumptions it is not necessary to discuss them explicitly.

It suffices to say that in the worst cases this may

introduce an error of 1% in $\sqrt{V_2}$.

3. Typical calculations on this

quantity show that it can never introduce an error of as

much as 1%.

Thus far we have assumed that $\sqrt{V_1}$ is known which is

actually not the case. If we examine Equation 2-16 we

see that by knowing $\sqrt{V_1}$ and $\sqrt{V_2}$, it is possible

to calculate $\sqrt{V_3}$. Since, of course, $\sqrt{V_3}$ is not known,

it is necessary to approximate $\sqrt{V_3}$ by neglecting $\sqrt{V_2}$ in

Equation 2-16. If we neglect $\sqrt{V_2}$ and obtain $\sqrt{V_3}$ then

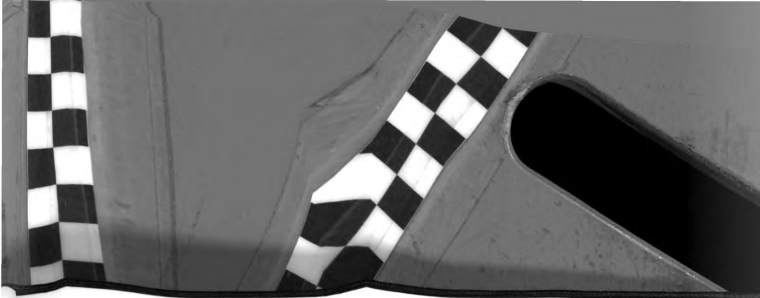
put this into Equation 2-17 to obtain an approximation

to $\sqrt{V_2}$. We can approach $\sqrt{V_2}$ by successive approx-

imations. For small values of $\sqrt{V_2}$ these corrections are

small and even for the largest values observed the error

is less than 10%.



Thus it appears that this method is susceptible, in the very worse cases, to errors of the order of 20 to 30%. According to Bloembergen⁶ the method of direct calculation of Q_c from known conductivities introduces errors as large as 30% in the total Q , which in turn results in values of u^i in error by a factor of three. It is possible to perform a normalization, similar to that which we have performed, which eliminates this error in part. If this is carried out the error in u^i is reduced to a maximum value of 25%. In this discussion we are considering only the error introduced in the evaluation of the data and not the systematic errors incurred in the experiment itself.

The temperature dependence of the saturation magnetization was obtained from data in Bozorth's²¹ book and the temperature dependence of the first order anisotropy constants was obtained from Mudar²².

There is apparent that this method is applicable in the very worst case, to errors of the order of 20 to 30%. According to the method of direct calculation of δ , from known systematic laboratory errors as large as 30% in the total δ , which is then revealed in values of δ in error by a factor of three. It is possible to reduce the systematic errors, which is that which we have achieved, which eliminates this error in part. In this is carried out the error in δ is reduced to a maximum value of 15%. In this discussion we are considering only the error introduced in the evaluation of the data and not the systematic errors inherent in the experiment itself.

The temperature dependence of the saturation magnetization was obtained from data in Borsanyi's book and the temperature dependence of the first order anisotropy constant was obtained from Nagai.



VI. RESULTS AND CONCLUSIONS

a. Nickel

Figure 11 shows a typical normalized resonance for electroplated nickel. The dotted line is plotted for $\mu'_{\infty} = 1$, the solid for μ'_{∞} evaluated by Equation 5-24. It is thus worth while in the interest of good fit to estimate μ'_{∞} from the first order approximation to the width and then replot the theoretical curve from this value. It is also obvious from the two curves that the difference in the line width and therefore in the value of $1/T_2$ is very slight, the correction obtained not being worth the effort in performing the multiple approximation in most cases.

Figures 12 and 13 show H_{ore} as a function of the angle between H and the crystallographic axes. These results are as predicted by theory except for the rather large anisotropy shift in H_{ore} in the (100) plane, corresponding to $K_1 = 55 \times 10^3$ ergs/cc. whereas the value obtained by Mudar on samples cut from the same rods using the torque magnetometer was about 46×10^3 ergs/cc. The broad resonance line and the consequent indeterminacy in H_{ore} may account for this difference. In addition the results further serve to establish the fact that the crystals have been properly oriented in the cutting.

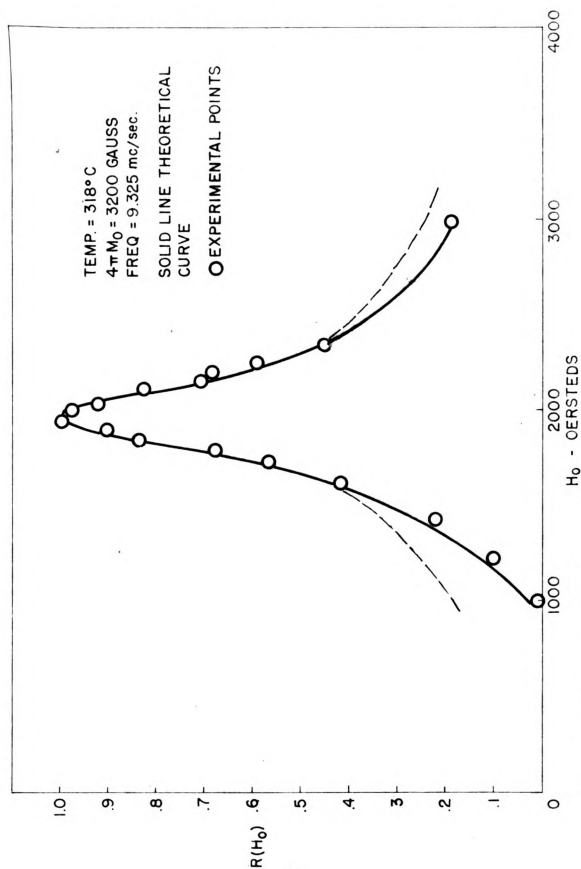


Figure 11 Normalized curve for electroplated nickel.

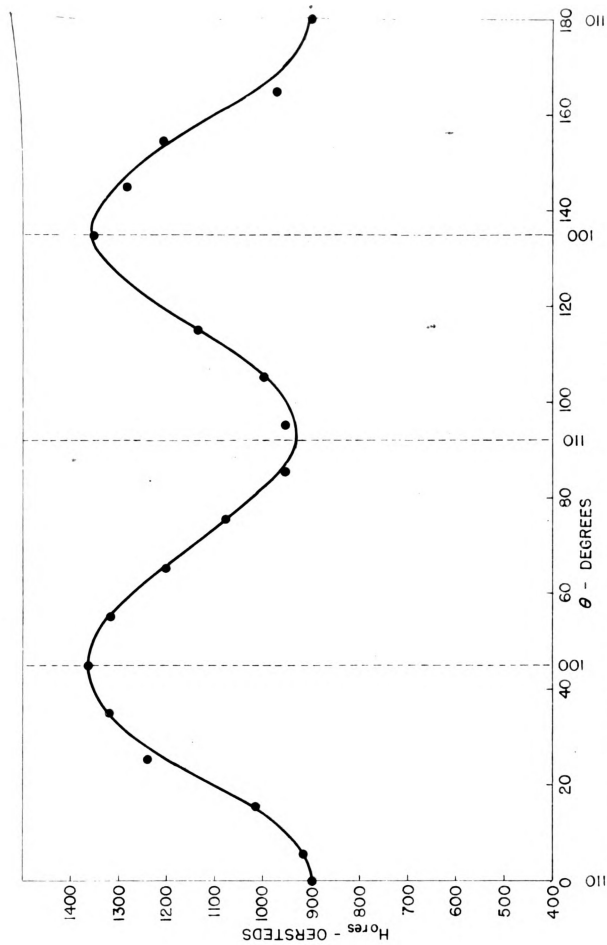


Figure 12 H_{res} as a function of angle in the (100) plane of nickel.

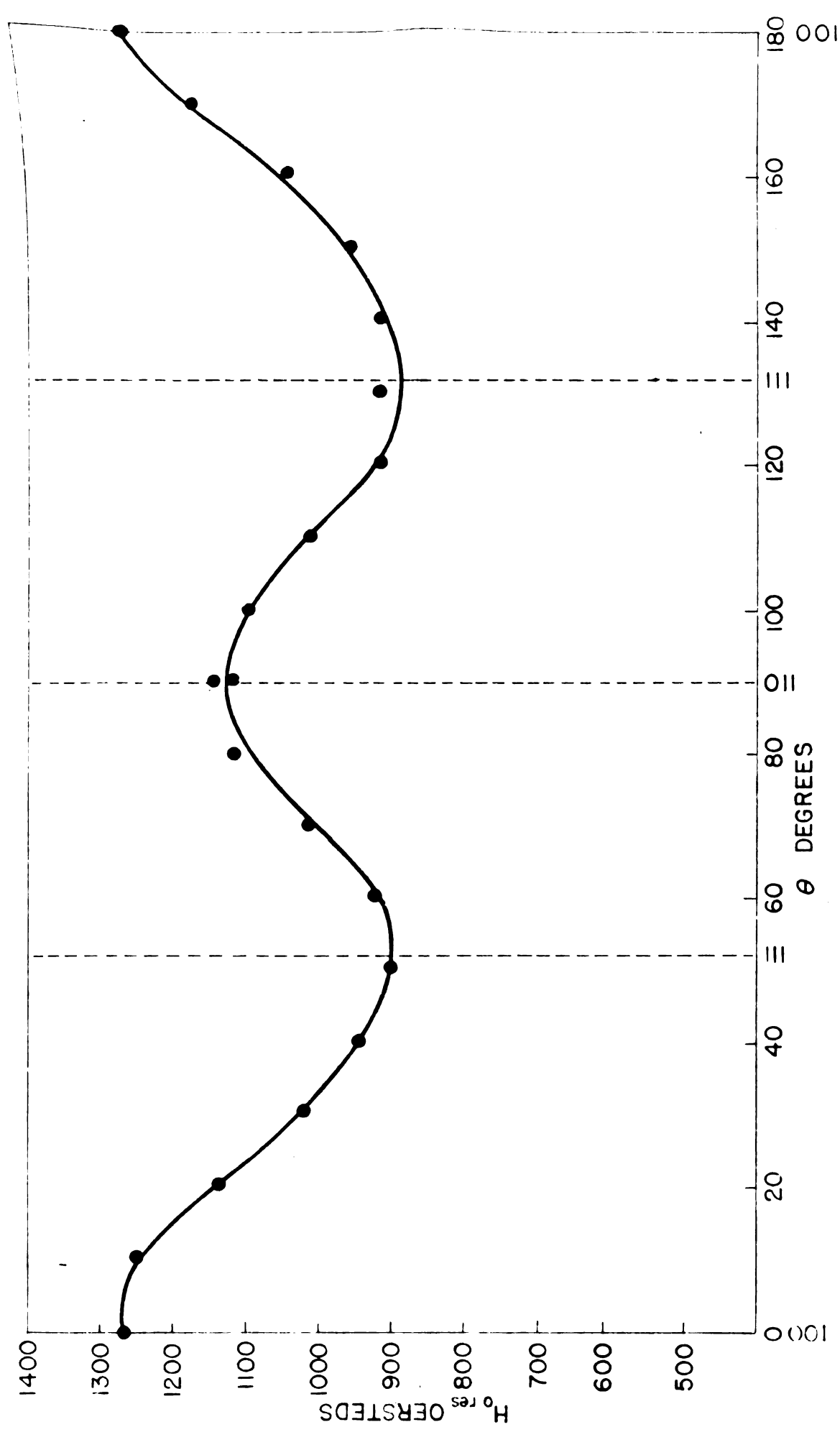


Figure 13. H_{0res} as a function of angle in the (110) plane nickel.

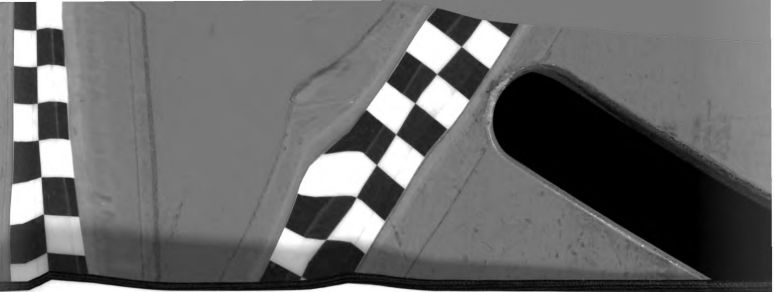


Figure 14 is a plot of $1/T_2$ as a function of temperature for various nickel samples. The results for the electroplated nickel are in agreement with those obtained by Bloembergen⁶ for polycrystalline sheets while the single crystal samples show anomalously large widths at room temperature. While the errors in the measurement of $1/T_2$ are very large (see Section VI. c) the difference between the values observed for single crystals and those for plated samples appear to lie within the experimental error. Furthermore the fact that the three curves agree quite well in the vicinity of the Curie point lends weight to the validity of the curves at lower temperatures. Based on a simple picture it is theoretically expected that the single crystal samples would have narrower widths. This is due to the random orientation of the microcrystals in the polycrystalline material with the result that the effective field acting on each microcrystal is a function of its orientation. The net effect is to broaden the applied field distribution over which resonance takes place.

There are at least two factors which could introduce erroneous values of $1/T_2$ in the experiment. The wider lines may be attributable to the possibility of strain broadening of the line. If all of the strains introduced in preparing the samples were not removed in polishing and etching, the decrease in $1/T_2$ with temperature might be explained as a partial relieving of those strains. If this were the case it might be expected that when the sample

Figure 1 is a plot of ΔT as a function of time - structure for various nickel samples. The results for the electroplated nickel are in agreement with those obtained by Bloembergen for polycrystalline sheets while the single crystal samples show anomalously large ΔT at room temperature. While the errors in the measurement of ΔT are very large (see section II.2) the difference between the values observed for single crystals and those for plated samples seems to lie within the experimental error. Furthermore the fact that the three curves agree quite well in the vicinity of the Curie point lends weight to the validity of the theory at lower temperatures. Based on a single crystal it is theoretically expected that the single crystal samples would have narrower widths. This is due to the random orientation of the microcrystals in the polycrystalline material with the result that the effective field acting on each microcrystal is a function of its orientation. The net effect is to broaden the applied field distribution over which resonance takes place. There are at least two factors which could introduce erroneous values of ΔT in the experiment. The wider lines may be attributable to the possibility of strain broadening of the line. If all of the strains introduced in preparing the samples were not removed in polishing and etching, the decrease in ΔT with temperature might be explained as a partial relief of these strains. If this were the case it might be expected that when the sample

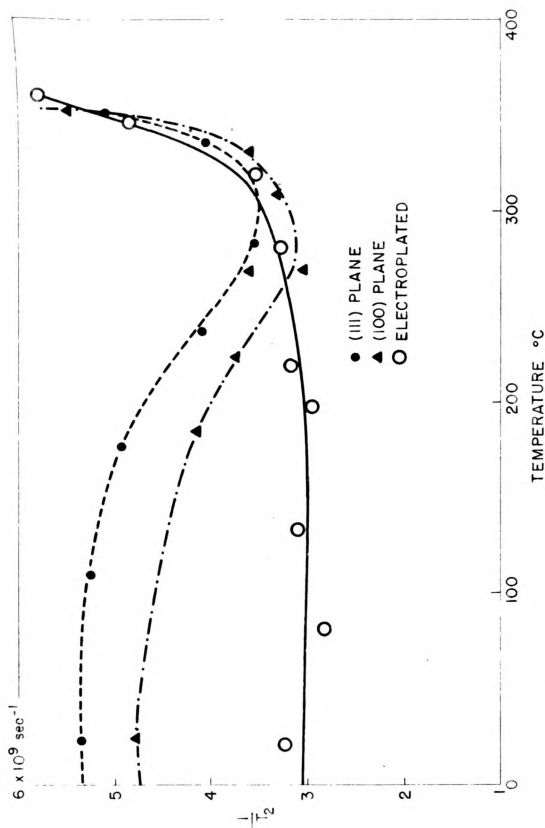
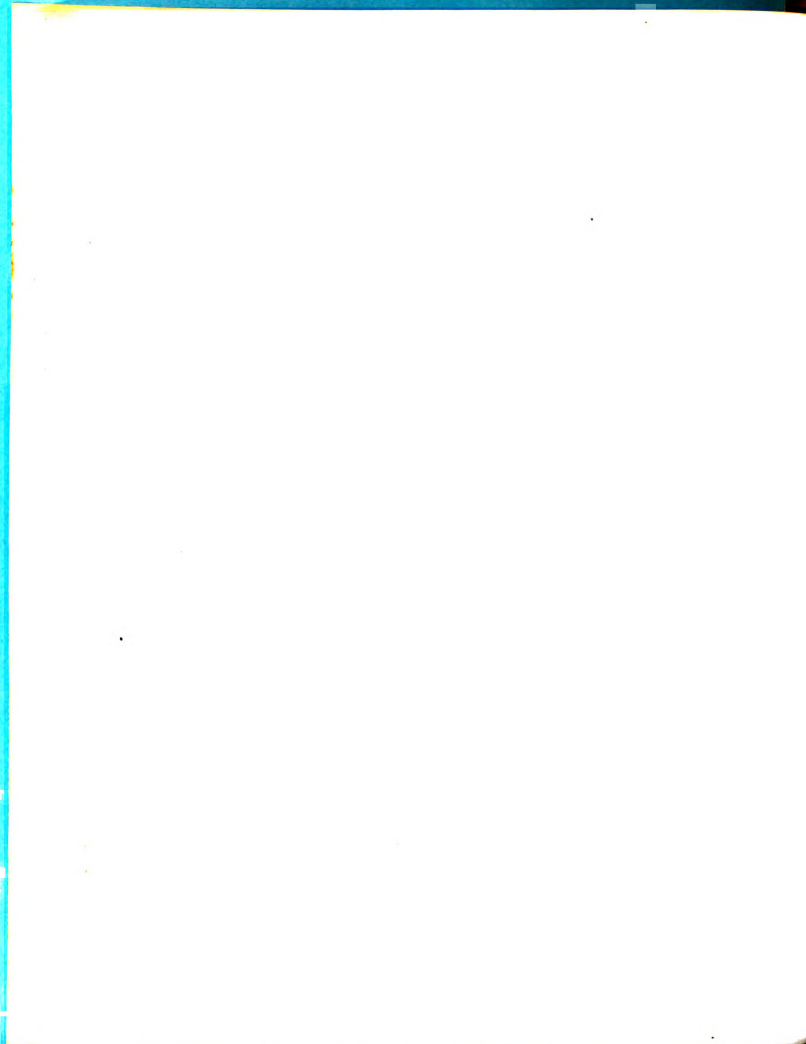
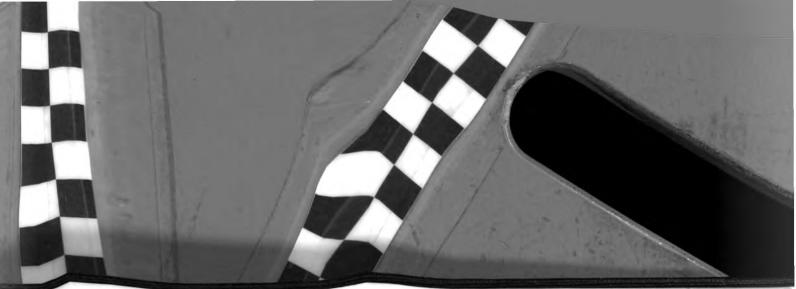


Figure 14 Temperature dependence of $\frac{1}{T_2}$ for nickel.

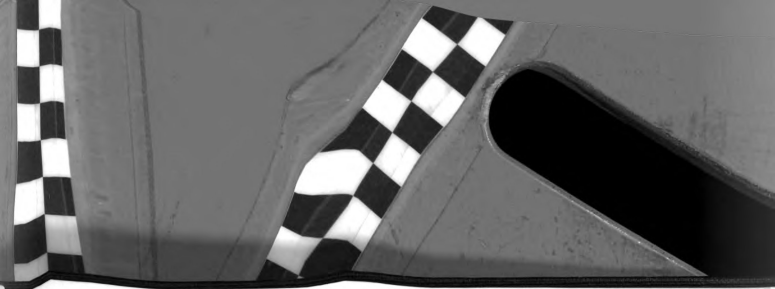




was returned to room temperature after heating the value of $1/T_2$ would be lower than before. This does not appear to be the case experimentally. It is also to be expected that if residual strains were responsible for this, room temperature data taken on many samples with differing types of preparation would give values of $1/T_2$ comparable in some cases to those of the plated sample. In no case was this true.

The other possible cause of wider lines in the single crystal samples is the method of mounting. Gaps between the edge of the sample and the plate in which it was imbedded could possibly distort the microwave field in such a way as to give high values of $1/T_2$. Qualitatively the effect might be described as follows. The gap causes a deformation in the radio frequency currents which are flowing in the end plate of the guide. This in turn causes a corresponding deformation in the magnetic field which could have had three effects:

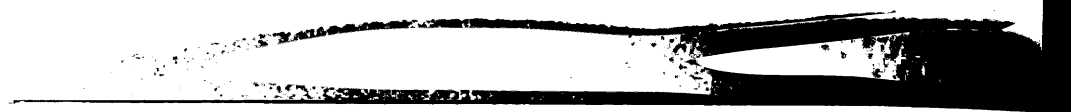
- 1) It decreased the magnitude of the effective H_{rf} in the plane of the sample and thus decreased the magnitude of the absorption.
- 2) It produced a distribution in the value of H_{rf} over the surface which in turn produced wider resonance lines.
- 3) It introduced an H_{rf} component perpendicular to the face of the sample which could have satisfied a different resonance condition.



The first effect should have no effect on either the position or width for a cavity of moderately high Q where the resonance position is a weak function of the losses. The second condition certainly will broaden the line but does not appear likely to shift it. The effect of the third condition is not immediately obvious but the normal field resonance²³ occurs in supermalloy, for example, at a field approximately three times the value for the parallel case. Thus one would expect that this could not perturb the resonance in this manner.

In connection with the problem of the effect of strains on line width, Figure 15 is a plot of $1/T_2$ versus strains in a 18% Co-Ni electroplated alloy. This material had a very narrow line width and appeared particularly suitable for making measurements of the effect of strains on line width. Strains were introduced in the form of scratches 7 microns wide passing through the plate and extending from one edge of the cone to the other. Two different dependences are plotted - the variation of $1/T_2$ with the number of scratches with the microwave magnetic field (1) parallel to the scratches and (2) perpendicular to the scratches. The variation with orientation indicates that the effect of field distortion is as large as that of strain.

If crystals of nickel large enough to cover the entire end of the waveguide had been available, the question of field distortion could have been resolved. However,



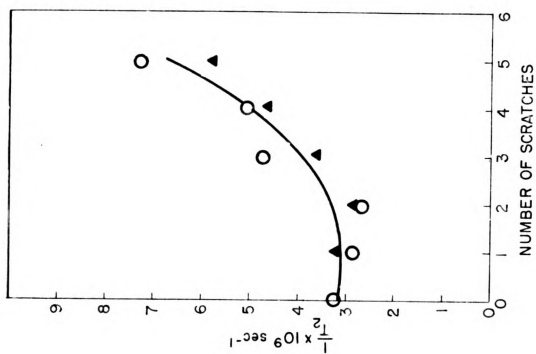


Figure 15. $1/t_2$ vs. number of scratches
18% Co-Ni plated alloy.
○ Scratch parallel to H_0
▲ Scratch perpendicular to H_0

results with a large iron sample which did cover the entire end of the guide suggest that such gaps around the edge of the sample were probably unimportant in this experiment. There are other possibilities such as the fact that the data on M_0 was obtained from other authors which might explain the results. However, none of these appear very likely.

Figure 16 is a plot of the g values of nickel as a function of temperature for the same samples as were used in Figure 14. A g value of 2 represents the case where the magnetic moment is due only to the spin angular momentum of the electron. Values larger than 2 indicate contributions from the orbital angular momentum. The decrease in the g value as the temperature increases should indicate a decrease in the coupling between the spin and orbit systems. The actual observed g value is very sensitive to both the resonance field and the magnetization and therefore at high temperatures is strongly dependent on accurate determination of both temperature and magnetization. It therefore seems possible that the g value may actually remain constant as found by Bloembergen⁶.

b. Iron

Figures 17 and 18 are plots of H_0 res as function of sample orientation in armco iron. $\cos 4\theta$ is also plotted in Figure 17. Several things differ from similar



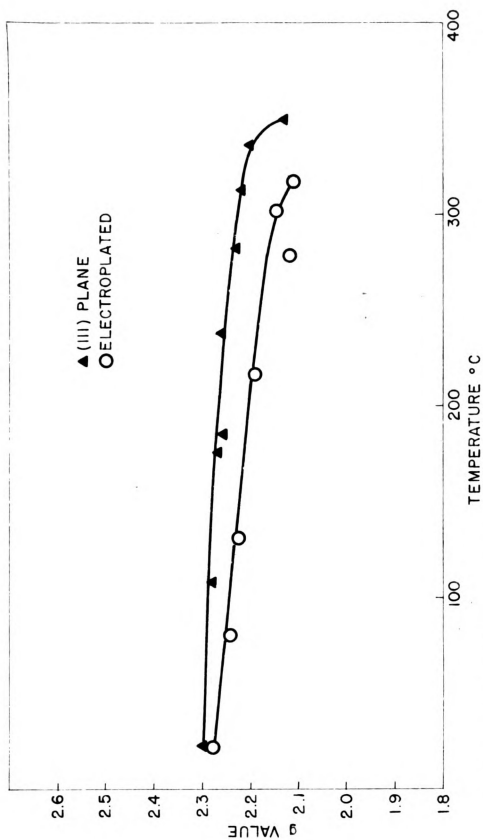
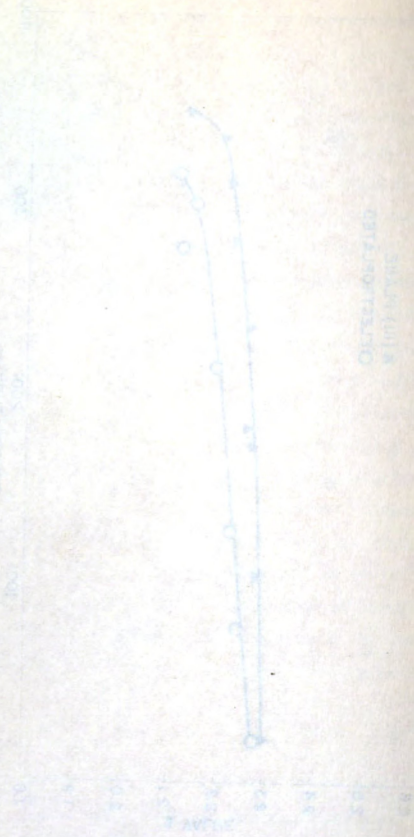


Figure 16. g values for nickel.

TABLE 1. SUMMARY OF DATA

TABLE 1. SUMMARY OF DATA



CURVE OF WIND VELOCITY

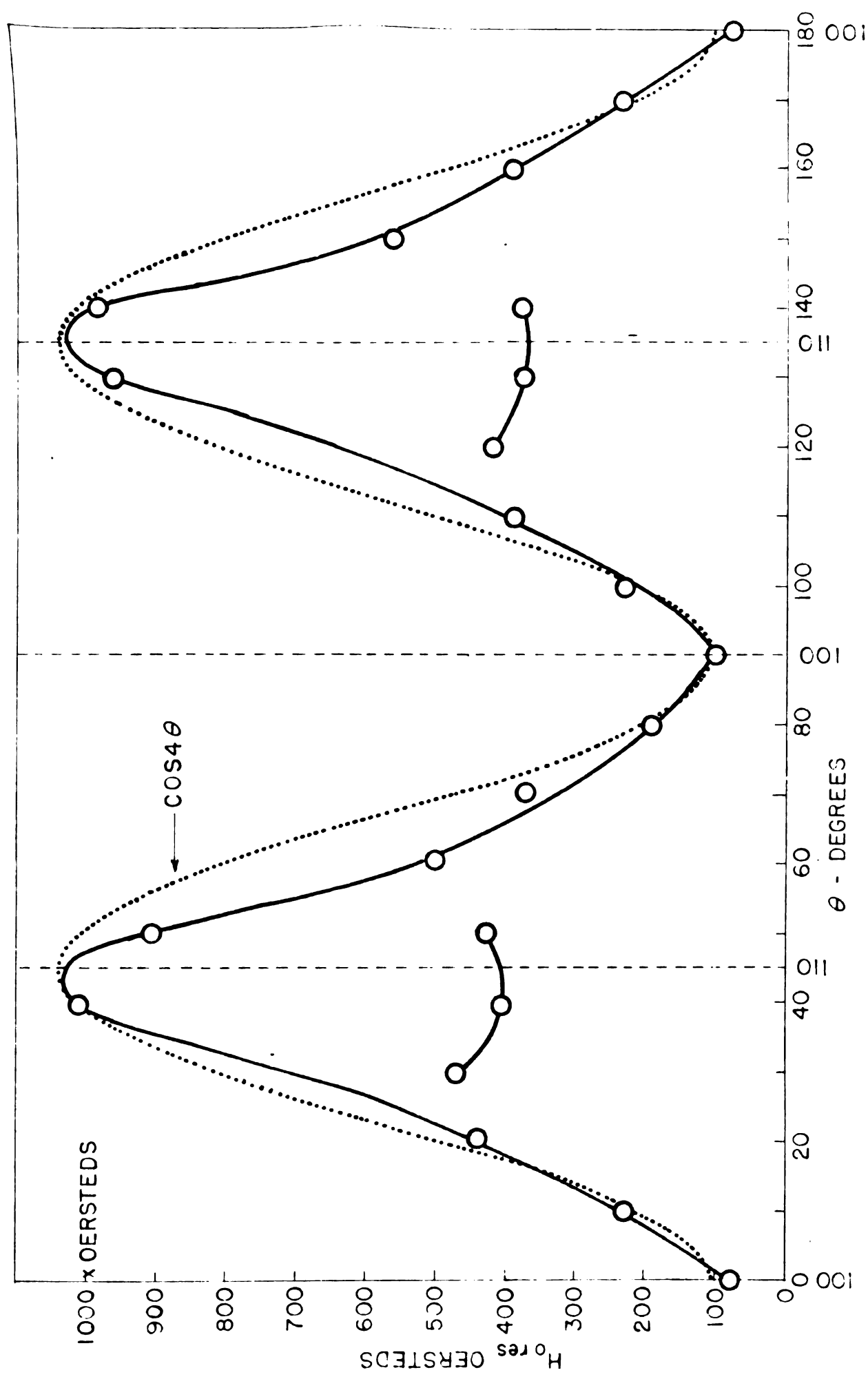
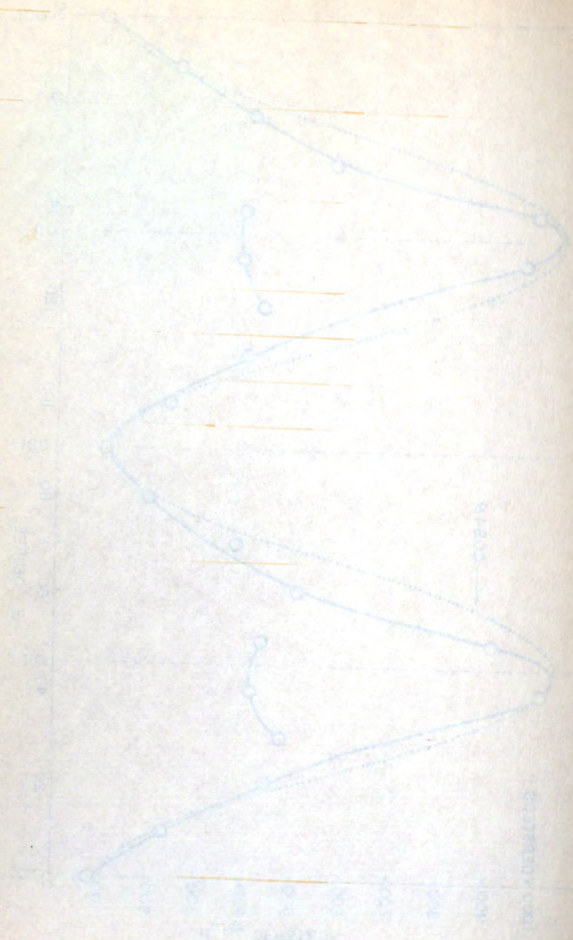


Figure 17. H_{ores} as a function of angle in the (100) plane of iron.

Graph 11. The variation of the ratio of the area of the peak at 100% to the area of the peak at 100%.



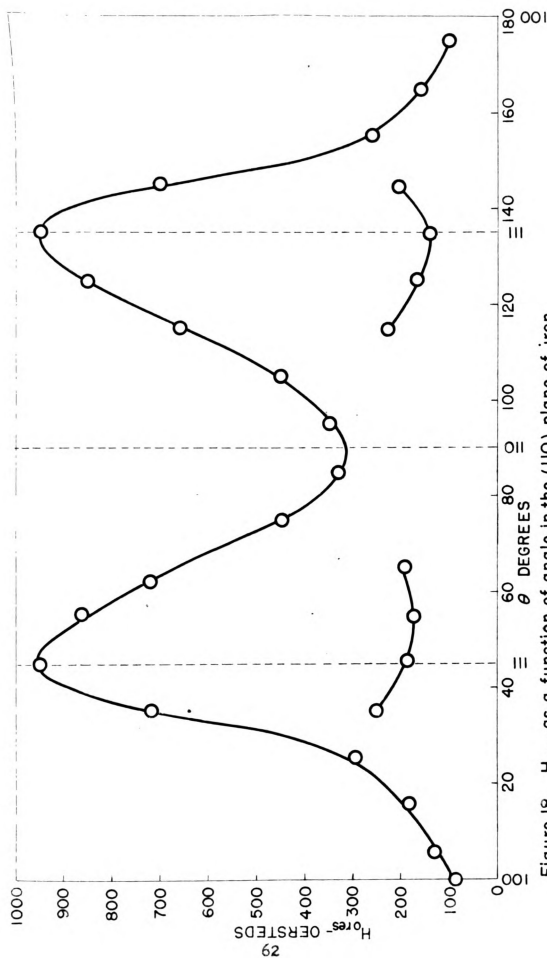
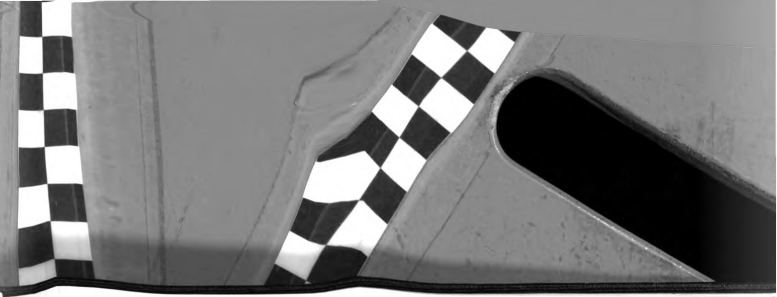
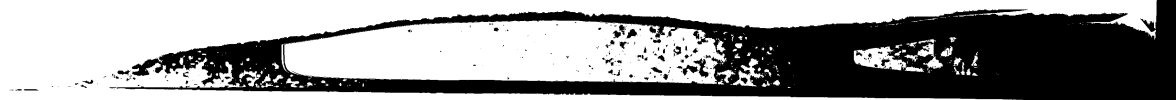
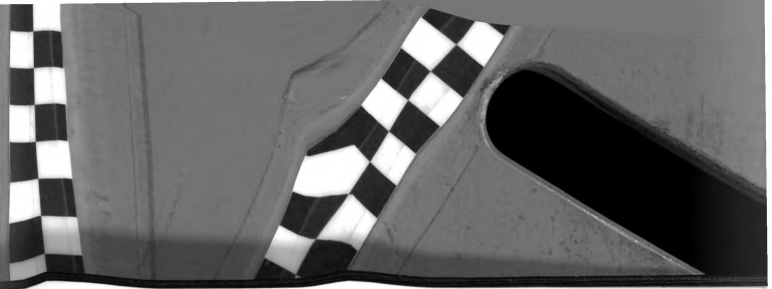


Figure 18. H_{ores} as a function of angle in the (110) plane of iron.



data taken by Kip and Arnold. The deviation from a $\cos 4\theta$ is not so symmetric as theirs. H_0 res of the secondary peak increases as the direction of the applied field moves away from the hard toward the easy direction of magnetization - their secondary peak position was an inverted function of θ . The plots do not show this, but in many cases the position of the primary peak seemed perturbed by the presence of the secondary peak; thus, at about 60° and 25° on Figure 17 it is difficult to determine whether there are two peaks or only one and if so, what the position of this peak is. Even at 30° it is almost impossible to locate the position of the primary peak. In iron as in nickel there was no anisotropy observed in the (111) plane so that the second order anisotropy constant was dropped from all calculations. In order to obtain a simple resonance type curve which was amenable to the analysis, it was necessary to have a sample cut from the (111) plane or to, in the case of samples cut from other planes, orientate the sample with respect to H_0 so that the anisotropy torque was minimized. If this was not done the resonance curves showed double peaks which could not be analysed. These double peaks were first observed by Kip and Arnold in experiments done at 9000 megacycles per second but not in similar ones at 24,000 megacycles per second. They also noted that the dependence of the primary peak was not at $\cos 4\theta$ as predicted by theory (Equation 2-20).





They attributed both of these phenomena to the fact that the anisotropy torque prevented the magnetization vector from aligning itself parallel to the applied field. Thus the relatively low fields needed for resonance at 9000 megacycles per second exert torques on M which are weak compared to the anisotropy effects whereas at 24,000 megacycles per second the high resonance fields override anisotropy. Consider Figure 19 which might be a typical configuration for small applied fields. θ is the angle between the applied field H_0 and the crystal axes and α is the angle between M and the axes. Thus the effective field causing resonance is not H_0 but $H_0 \cos \beta$ and the angle for which the anisotropy correction to the resonance field is to be calculated is not θ but α . Thus it is possible, as H_0 increases, that there will be a value of α and $H_0 \cos \beta$ such that the resonance condition will be satisfied producing a low field 'secondary peak'. As H_0 is increased, α approaches θ and H_0 and θ will satisfy the resonance condition giving rise to the 'primary' or normal peak. Therefore in materials with strong anisotropy two peaks may occur. It is just because the anisotropy constant of nickel is one-third of that in iron that no double peaks are observed in nickel.

The temperature dependence of the double peaks is plotted in Figure 20. The two cuts show similar temperature dependence and both show that the secondary peak disappears as K_1 approaches zero.

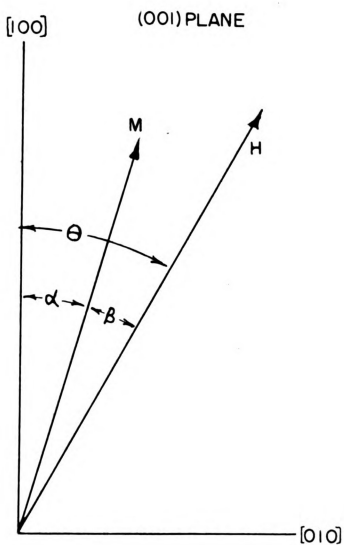
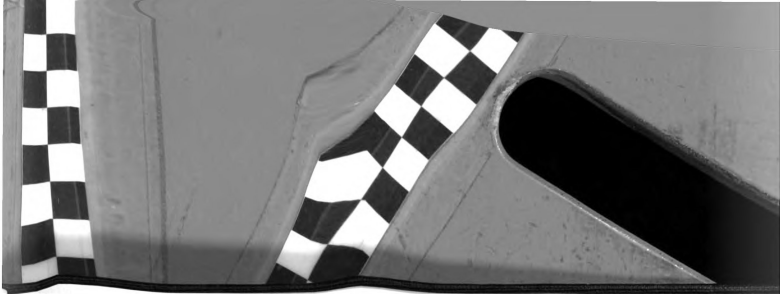
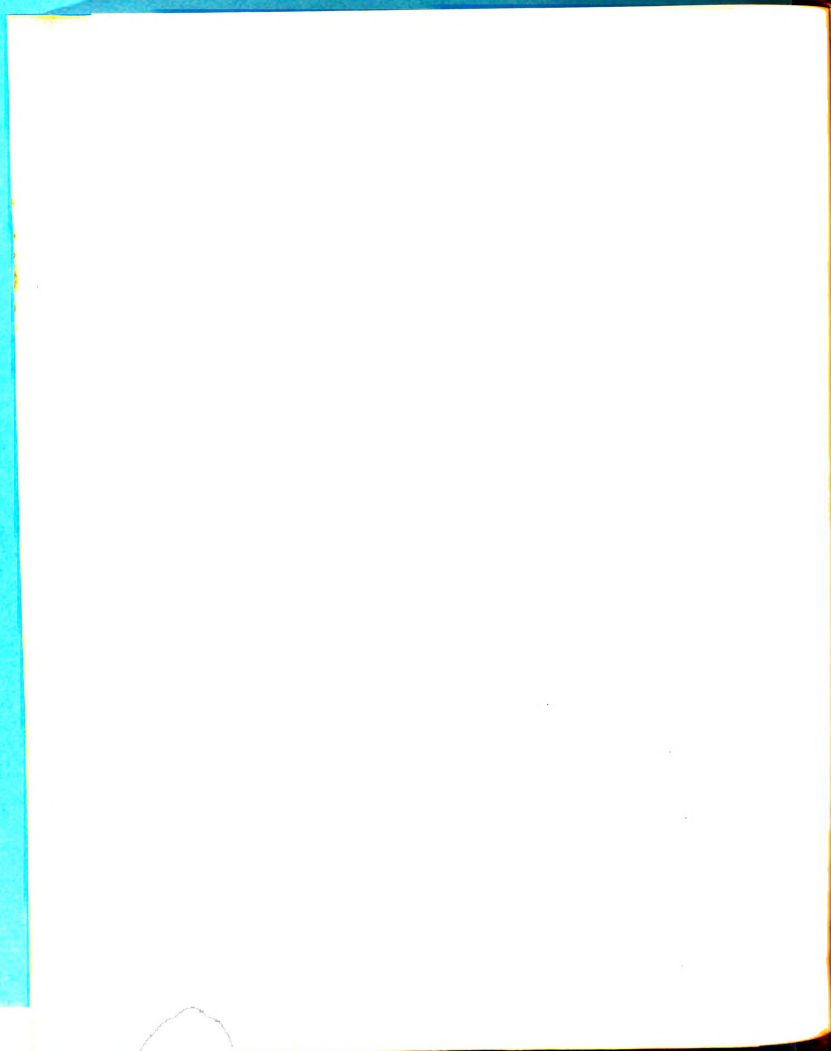


FIG. 19 DIAGRAM ILLUSTRATING EFFECT
OF ANISOTROPY TORQUE AT LOW
APPLIED FIELDS



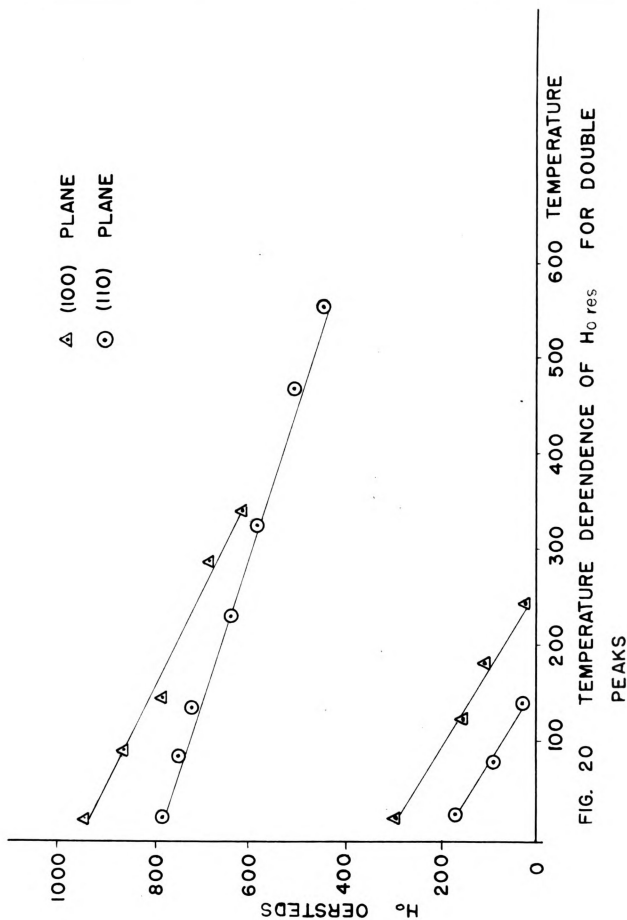


FIG. 20 TEMPERATURE DEPENDENCE OF H_0 res FOR DOUBLE PEAKS

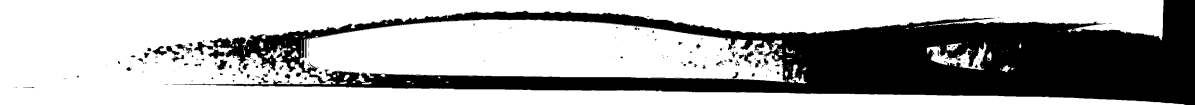




Figure 21 is a plot of $1/T_2$ as a function of temperature for two different iron samples - a (111) cut of armco iron and a sample cut from a sheet of grain oriented 3% Si-Fe in which the plane of the sample was the (110) plane. The polycrystals were of the order of .050" in diameter. Experiments done in this laboratory²⁴ show that the anisotropy constant of this material is approximately 70% of that for single crystals of similar composition. Significant data was obtained with only one sample of each material because of the difficulty of achieving temperatures as high as 800°C. The temperature dependence in the two cases is essentially the same although the line width is approximately 20% lower in the polycrystalline material. This may well be due to the fact that the rolled material is carefully annealed in manufacture and no further strains are introduced in the preparation while the sawing and polishing of the armco iron apparently introduces a few strains which are never removed. It is also possible that the purity of the iron has a large effect on the line width but the small amount of data which was taken does not confirm or deny this hypothesis. Since the oriented sample covered the entire end of the waveguide there was no possibility of the gap effect for this sample and the fact that the temperature dependence of $1/T_2$ is of the same form for the oriented and single crystal samples indicates that such a gap effect if it exists does not change the general shape of the curves. This conclusion in addition

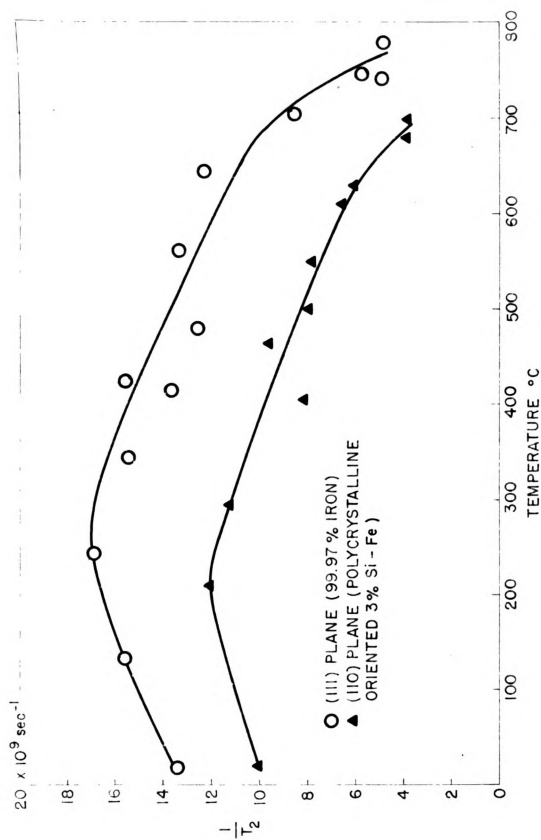
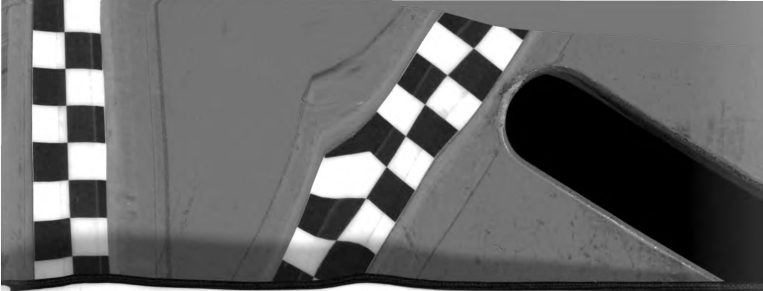


Figure 21. Temperature dependence of $\frac{1}{T_2}$ for iron.

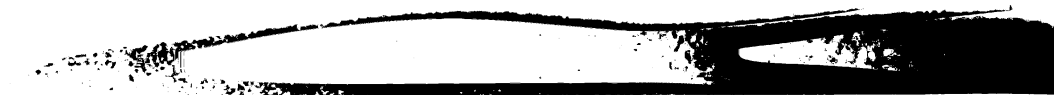


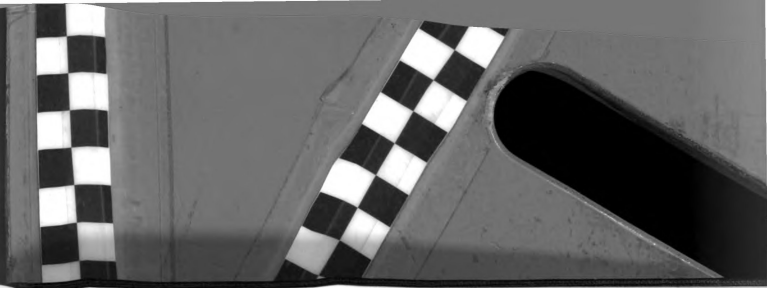
to the fact that $1/T_2$ definitely decreases as the temperature approaches the Curie point seems to lend weight to the curves observed for nickel single crystals.

c. Conclusions

In order to evaluate the results discussed in the previous two sections, it is necessary to investigate the sources of experimental error. Such things as meter inaccuracy, non-linearity of the amplifier, magnet hysteresis and deviation of the crystal from square law response may all be lumped together with a composite error of about 5%. The meters were accurate to 2% of full scale reading. The amplifier was determined to be linear to within the same 2%. Magnet hysteresis could be minimized by careful taking of data, and the typical crystal does not deviate from square law response by more than 2%.

The error introduced by mismatching in the guide is larger far from resonance where the standing wave ratio in the arm containing the cavity is low - near resonance the effect is small. Fortunately the portion of the resonance curve which determines $1/T_2$ lies in the 'near resonance' region. Thus 5% should be a very reasonable error in the worst cases. The temperature was measured to within 2°C at low temperatures, but the deviation was probably considerably higher at high temperatures. This is unfortunate since the error is much





more significant at high temperatures where the saturation magnetization varies most rapidly with temperature. Both the resonance position and the line width are dependent on the saturation magnetization and therefore the error introduced by inaccurate temperature measurement is probably as large as 15%.

Thus the overall error introduced experimentally can be estimated to be of the order of 25% in the very worst cases. This certainly appears to be a large error - and it may be that the estimate is larger than the experiment warrants - particularly when one recalls that microwave methods are currently giving us some of our most precise measurements. This, though, is typical of the accuracy generally obtainable in ferromagnetic resonance line width experiments, particularly at high temperatures.

Even allowing for the maximum error at all temperatures (which is not particularly reasonable) the general form of the line width curves (Figs. 14 and 21) appears valid.

Assuming that these experimental results are valid, it is only natural to ask how they compare with the current theory of line width. This question has no answer because there is no satisfactory theory of line width. In Section I we mentioned that Kittel¹⁴ had made calculations on the temperature dependence of the spin-spin relaxation time using the spin wave technique,

more significant to the experimental error than the error
 of the magnetic field. The error in the magnetic field
 is not negligible, but it is not the same as the error
 in the temperature. The error in the temperature is
 dependent on the type of thermometer used. The error
 in the magnetic field is dependent on the type of
 magnet used. The error in the temperature is
 dependent on the type of thermometer used.

There are several error factors which experimentally
 can be estimated. The error in the magnetic field
 is not negligible, but it is not the same as the error
 in the temperature. The error in the temperature is
 dependent on the type of thermometer used. The error
 in the magnetic field is dependent on the type of
 magnet used. The error in the temperature is
 dependent on the type of thermometer used.

Even if the error in the magnetic field is not
 negligible, it is not the same as the error in the
 temperature. The error in the temperature is
 dependent on the type of thermometer used. The error
 in the magnetic field is dependent on the type of
 magnet used. The error in the temperature is
 dependent on the type of thermometer used.

Assuming that these experimental results are valid,
 it is only natural to ask how they compare with the
 current theory of the effect. This question has no
 answer because there is no satisfactory theory of the
 effect. In Section I we mentioned that Kivel¹⁴ had
 made calculations on the temperature dependence of the
 spin-spin relaxation time using the spin wave technique.

and had suggested that at high temperatures this might be the dominant factor in line width. In that article he said:

... it is only recently that we have recognized what seem to be the real mechanisms causing the widths. A number of somewhat superficial mechanisms were explored without success in the early phases of research on ferromagnetic resonance.

Very recently Bloembergen²⁵, reporting on work at high microwave power levels which was undertaken with the same aim as the present work said the following:

... Even if Kittel's explanation for the width is accepted, his theory could not explain other experimental observations. Our results show that the inverse width [our $1/T_2$] cannot be identified with the spin-spin relaxation time.... The cause for the combined effects of the magnitude and temperature dependence of the spin-spin relaxation time and the value of the line width at low temperatures remains obscure.

And as a conclusion:

The present experiments, which were undertaken to clarify some of the issues of ferromagnetic relaxation, have only created new problems in this respect. An important point still seems to be missing in the theory below the Curie temperature.

It appears that we have no choice but to accept Bloembergen's statements as representing the present state of the theory, and to hope that further experimental results, including those represented by this work, will add sufficiently to our knowledge to enable us to formulate a more satisfactory theory of line width.

and had suggested that it was possible this might be the desired factor in the case of the first analysis he said:

... it is only possible that we have reached what now is a real equilibrium between the various factors. It is not possible in the early stages of reaction to reach a definite equilibrium.

Very recently, however, according to work at high altitudes, where lower air is maintained with the same air as the present work, the following:

... based on the equilibrium for the which is necessary, this theory is not certain other experimental observations. The results show that the theory is not correct. It cannot be identified with the equilibrium of the reaction and for the equilibrium of the reaction and the equilibrium of the reaction. The equilibrium of the reaction is not the same as the equilibrium of the reaction.

And as a result:

The theory of the reaction, which was undertaken to explain some of the results of the reaction, is not correct. It is only a theory and it is not a fact. It is only a theory and it is not a fact. It is only a theory and it is not a fact.

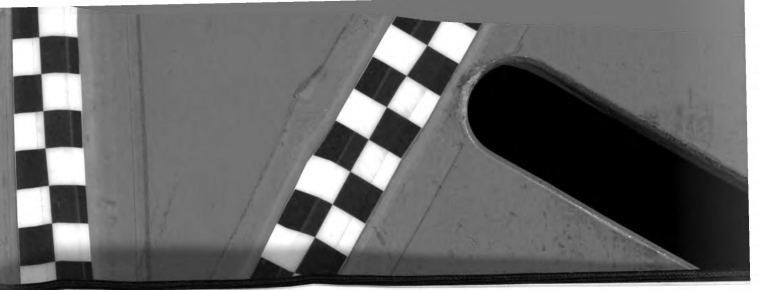
It appears that we have no choice but to accept the present theory as representing the present state of the theory, and to hope that further experimental results, including those represented by this work, will add sufficiently to our knowledge to enable us to formulate a more satisfactory theory of the reaction.



REFERENCES CITED

1. Griffiths, J.H.E. Anomalous High-frequency Resistance of Ferromagnetic Metals. Nature 158, 670 (1946)
2. Yager, W.A., and Bozorth, R.M. Ferromagnetic Resonance at Microwave Frequencies. Physical Review 72 80 (1947)
3. Kip, A.F., and Arnold, R.D. Ferromagnetic Resonance at Microwave Frequencies in an Iron Single Crystal Physical Review 75, 1556 (1949)
4. Yager, W.A., and Merritt, F.R. Ferromagnetic Resonance Absorption in Heusler Alloy. Physical Review 75, 318 (1949)
5. Kip, A.F., and Kittel, C. Microwave Resonance Absorption in Gadolinium Metal. Physical Review 82, 518 (1953)
6. Bloembergen, N., On the Ferromagnetic Resonance in Nickel and Superalloy Physical Review 78, 572 (1950)
7. Bickford, L.R. Jr. Ferromagnetic Resonance Absorption in Magnetite Single Crystals Physical Review 78, 449 (1950)
8. Okamura, T., Torizuka, Y., and Kojima, V. Ferromagnetic Resonance in Cobalt Ferrite at High Temperatures Physical Review 84, 372 (1951)
9. Okamura, T., and Kojima, V. Ferromagnetic Resonance in Single Crystals of Cobalt Zinc Ferrite Physical Review 85, 690 (1952)
10. Healy, D.W. Jr. Ferromagnetic Resonance Absorption in NiOFe_2O_3 as a Function of Temperature Physical Review 86, 518 (1953)
11. Kittel, C. On the Theory of Ferromagnetic Resonance Absorption Physical Review 73, 155 (1948)
12. Van Vleck, J.H. Concerning the Theory of Ferromagnetic Resonance Absorption Physical Review 78, 266 (1950)
13. Bloch, F. Nuclear Induction Physical Review 70, 460 (1946)

1. Smith, J. W. The Theory of Permanent Resonance
of Permanent Resonance. Physical Review 73, 370 (1946)
2. Yeh, K. H. and Yeh, K. H. The Theory of Permanent Resonance
of Permanent Resonance. Physical Review 73, 370 (1946)
3. Yeh, K. H. and Yeh, K. H. The Theory of Permanent Resonance
of Permanent Resonance. Physical Review 73, 370 (1946)
4. Yeh, K. H. and Yeh, K. H. The Theory of Permanent Resonance
of Permanent Resonance. Physical Review 73, 370 (1946)
5. Yeh, K. H. and Yeh, K. H. The Theory of Permanent Resonance
of Permanent Resonance. Physical Review 73, 370 (1946)
6. Yeh, K. H. and Yeh, K. H. The Theory of Permanent Resonance
of Permanent Resonance. Physical Review 73, 370 (1946)
7. Yeh, K. H. and Yeh, K. H. The Theory of Permanent Resonance
of Permanent Resonance. Physical Review 73, 370 (1946)
8. Yeh, K. H. and Yeh, K. H. The Theory of Permanent Resonance
of Permanent Resonance. Physical Review 73, 370 (1946)
9. Yeh, K. H. and Yeh, K. H. The Theory of Permanent Resonance
of Permanent Resonance. Physical Review 73, 370 (1946)
10. Yeh, K. H. and Yeh, K. H. The Theory of Permanent Resonance
of Permanent Resonance. Physical Review 73, 370 (1946)
11. Yeh, K. H. and Yeh, K. H. The Theory of Permanent Resonance
of Permanent Resonance. Physical Review 73, 370 (1946)
12. Yeh, K. H. and Yeh, K. H. The Theory of Permanent Resonance
of Permanent Resonance. Physical Review 73, 370 (1946)
13. Yeh, K. H. and Yeh, K. H. The Theory of Permanent Resonance
of Permanent Resonance. Physical Review 73, 370 (1946)

- 
14. Abrahams, E., and Kittel, C. Relaxation Processes in Ferromagnetism Reviews of Modern Physics 25, 233 (1953)
 15. Kittel, C., and Abrahams, E. Dipolar Broadening in Magnetically Dilute Crystals Physical Review 90, 238 (1953)
 16. Bloembergen, N. On the Magnetic Resonance Absorption in Conductors Journal of Applied Physics 23, 1383 (1952)
 17. Osborne, J.A. Demagnetizing Factors of the General Ellipsoid Physical Review 67, 351 (1945)
 18. Jaquet, P. Electrolytic Polishing of Copper Comptes Rendues 202, 403 (1936)
 19. Elmore, W.C. Electrolytic Polishing Journal of Applied Physics 10, 724 (1939)
 20. McKeehan, L.W. and Elmore, W.C. Surface Magnetization of Ferromagnetic Crystals I and II Physical Review 46, 226 and 529 (1934)
Elmore, W.C. Ferromagnetic Colloid for Studying Magnetic Structures Physical Review 54, 309 (1938)
 21. Bozorth, R.M. Ferromagnetism (D.Van Nostrand Co. New York 1951)
 22. Mudar, J. Unpublished M.S. Thesis, Michigan State College (1953)
 23. Kittel, C. On the Gyromagnetic Ratio and Spectroscopic Splitting Factor of Ferromagnetic Substances Physical Review 76, 743 (1949)
 24. Morrison, C.A. Unpublished M.S.Thesis, Michigan State College (1952)
 25. Bloembergen, N., and Wang, S. Relaxation Effects in Para- and Ferromagnetic Resonance Physical Review 93, 72 (1954)





MICHIGAN STATE UNIV. LIBRARIES



31293017640339